

Physical Properties of the Particles Composing the Martian Dust Storm of 1971-1972

OWEN B. TOON¹

Laboratory for Planetary Studies, Cornell University, Ithaca, New York 14853

JAMES B. POLLACK

*Theoretical and Planetary Studies Branch, Ames Research Center, NASA,
Moffett Field, California 94035*

AND

CARL SAGAN

Laboratory for Planetary Studies, Cornell University, Ithaca, New York 14853

Received May 14, 1976; revised September 9, 1976

Infrared spectra obtained from the Mariner 9 spacecraft during the 1971-1972 dust storm are used to derive information on the composition and particle size distribution of the dust and to study the time evolution of the storm. The dust is not composed of pure granite, basalt, basaltic glass, obsidian, quartz, andesite, or montmorillonite. The infrared spectra suggest that the dust is a mixture of materials, dominated by igneous silicates with >60% SiO₂, or weathering products such as clay minerals, but the dust could possibly have a significant component of lower SiO₂ materials such as basalt. Substantial quantities of carbonates, nitrates, or carbon suboxide are excluded from the mixture. All infrared, visible, and ultraviolet data on the Martian surface composition seem consistent with a mixture of basalt and clay minerals or high SiO₂ igneous rocks, with a surface patina of oxides of iron. For all candidate compositions, the data are best matched with a size distribution that approximates a differential power law function of slope -4. This size distribution is quite similar to terrestrial size distributions in regions remote from sources of dust. The relative abundance of particles between 1- and 10- μ m radius did not change during the Mariner 9 mission; thus suspended particles did not experience Stokes-Cunningham fallout but instead were supported by turbulence with an eddy diffusion coefficient, $K_e \approx 7 \times 10^6 \text{ cm}^2 \text{ sec}^{-1}$. The aerosol optical depth, standardized to 0.3- μ m wavelength, varied from about 1.5 early in the mission to about 0.2 at Orbit 200.

INTRODUCTION

A unique opportunity to study natural dust particles was provided by the infrared interferometric spectrometer (IRIS) on the Mariner 9 spacecraft which observed a global Martian dust storm during 1971-2 (Hanel *et al.*, 1972a, b, c; Conrath

et al., 1973). Since the dust particles were suspended as a fine cloud, their infrared features were much stronger and more distinct than the compacted powder emission features typical of a planetary surface. Moreover, multiple scattering in a dust cloud is a tractable theoretical problem while scattering in a compacted powder is not. On Earth, strong gaseous absorption prevents us from making *in situ* infrared

¹Current address: Theoretical and Planetary Studies Branch, Ames Research Center, NASA, Moffett Field, Calif. 94035.

TABLE I
Properties of Data from IRIS^a

Revolution	Surface pressure (mb)	Mean view angle (deg)	Spread of view angle (deg)	Approximate brightness temp. deviation (°K)	Number of spectra averaged
8	4.5	65.3	2	2	5
56	4.5	25.3	3	1	6
72	4.7	14.4	4	1	7
80	4.8	66.6	2	2	3
138	4.7	5.2	5	1	12
146	4.4	10.9	5	1	9
154	4.7	58.2	3	1	5
206	4.7	13.0	2	3	6

^a All data were taken in the region bounded by -20 to -40° latitude and 250 to 190° longitude.

spectra of natural aerosols in many spectral regions, but on Mars, gases are important only in limited spectral regions so *in situ* studies are feasible. For these reasons, the Martian dust-storm observations merit careful study.

There have been several previous studies of the IRIS spectra. Hanel *et al.* (1972c) qualitatively compared the IRIS spectra with laboratory spectra and concluded that the dust could be igneous rock with an SiO_2 content of $60 \pm 10\%$. Hunt *et al.* (1973) also made qualitative comparisons and suggested that the dust might be composed of the clay mineral montmorillonite. Although qualitative comparisons provided valuable information, Conrath *et al.* (1973) recognized that quantitative calculations were necessary to obtain more detailed information. They performed such calculations for quartz and deduced that quartz could not be the dominant dust-cloud component and that the particles causing the observed IRIS spectra had radii between 1.0 and $10.0 \mu\text{m}$. Most recently, Aronson and Emslie (1975) performed quantitative calculations for several minerals and rocks in which the effect of the nonspherical shape of the dust particles on the spectrum was considered. They concluded that the particles had diameters

of about $1 \mu\text{m}$ and may have been feldspar rich. The work presented here differs from the earlier studies in several ways. First, we include different materials. For example, we test Hunt *et al.*'s suggestion that montmorillonite might compose the dust. Second, we assume that the particles composing the dust are spherical. Thus, our work may be contrasted with that of Aronson and Emslie to determine if particle shape affects conclusions drawn from the IRIS spectra. Third, we study the particle size in detail and make estimates of the particle size distribution. Finally, we analyze spectra from orbits spread throughout the Mariner 9 mission to study the time dependence of the dust properties.

Below we first describe the data available to us and our method of analyzing it. Next we examine the ways in which the optical properties of dust cause the observed spectra. This knowledge allows us to deduce the kind and amount of information that can be obtained from an observed spectrum. Then we analyze the IRIS spectra of the Martian dust storm to find the dust optical depth, composition, and size distribution. Finally, we consider the implications of the results of the analysis for the geology and meteorology of Mars.

DATA AND TECHNIQUE OF ANALYSIS

High-quality spectra from 200 to 2000 cm^{-1} were obtained by the infrared interferometric spectroscopy experiment on the Mariner 9 spacecraft. The IRIS experimenters kindly provided us with spectra selected to maximize their usefulness for our study. To improve the signal/noise ratio, several spectra acquired from similar view angles on the same spacecraft orbit were averaged to produce a mean spectrum. Mean spectra from different orbits were obtained from a restricted location with uniform surface pressure to minimize variation with position on the Martian surface. All the spectra were obtained near the subsolar point to enhance the temperature difference between the atmosphere and the ground and thereby improve spectral contrast. Table I summarizes the properties of the spectra. The IRIS experimenters also provided us with vertical temperature profiles for each orbit. These were obtained from analysis of the observed emergent intensity in the 667-cm^{-1} CO_2 band (e.g., Conrath *et al.*, 1973).

We have generated theoretical spectra of the emergent intensity from dust clouds with properties similar to those of the Martian dust cloud. To the extent that our theoretical spectra are unambiguous and accurate, the dust-storm properties will be known when our theoretical spectra duplicate the observed spectra.

The emergent intensity from a homogeneous, plane-parallel atmosphere is (see Chandrasekhar, 1960)

$$I_\nu(0, +\mu, \theta) = I_\nu(\tau^*, +\mu, \theta)e^{-\tau^*/\mu} + \int_0^{\tau^*} e^{-t/\mu} S_\nu(t, +\mu, \theta) dt/\mu. \quad (1)$$

Here, τ^* is the total optical depth at frequency ν ; θ is the azimuth angle; $\arccos\mu$ is the view angle; $I_\nu(\tau^*, \mu, \theta)$ is the intensity of emitted light at the ground; and S_ν is the source function, which can

formally be defined using the scattering phase function, P_ν , the single scattering albedo $\bar{\omega}_{0\nu}$, and the Planck function, B_ν :

$$S_\nu(t, \Omega) = \int_{\Omega'} P_\nu(\Omega', \Omega) I_\nu(\Omega', t) (d\Omega'/4\pi) + (1 - \bar{\omega}_{0\nu}) B_\nu(t).$$

The first term, which is integrated over solid angle, represents scattering into the view angle and the second term represents emission from the dust particles. In Appendix A, we describe an approximate technique for calculating the source function that uses the two-stream solution to the equation of radiative transfer (Sagan and Pollack, 1967). Qualitatively, our approximation consists of replacing the phase function integral in the source function with the first two terms of a Gaussian

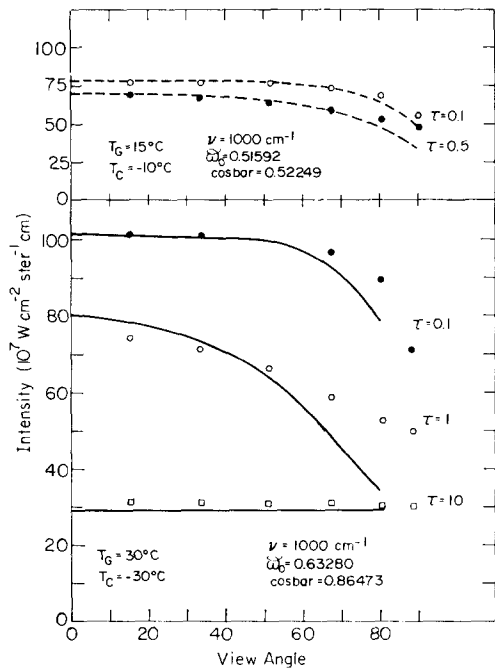


FIG. 1. The emergent intensity vs view angle for a haze (top) and a cloud (bottom). The curves are from precise calculations and the symbols are from approximate calculations of the present paper. The precise haze calculations were made by Liou (1973) and the precise cloud calculations by Yamamoto *et al.* (1966).

quadrature sum, and using the two-stream solutions to represent the scattered intensity field at the Gauss points. Conel (1969) anticipated that this would be a useful approximation, although it apparently has not been employed before now.

We have made several tests of the accuracy of our approximation. The solution for the emergent intensity becomes exact as $\bar{\omega}_0 \rightarrow 0$, and emission and absorption dominate. Curran *et al.* (1973) have made precise calculations of the emergent intensity from Martian water ice clouds and they generously provided us with numerical results for comparison. In a test case employing $\arccos \mu \simeq 0^\circ$, $\tau^* \simeq 0.3$, $\bar{\omega}_0 \simeq 0.2$, and $\bar{\cos} \mu \simeq 0.3$ (defined in Appendix A), the approximation method agrees with Curran's results to within 0.06°K in brightness temperature. For roughly the same conditions except with $\bar{\omega}_0 \simeq 0.9$ and $\bar{\cos} \mu \simeq 0.75$, the approximation is within 0.5°K of the correct value.

Under certain conditions, our approximation is not very accurate. The upward

and downward two-stream intensities are isotropic over their hemispheres. The angular dependence of intensity in our approximation arises from the difference in path length between different view angles, not because of angular dependence in the phase function; that is, with our approximation, μ appears in (1) in the exponential terms but not in the source function. For strongly forward-scattering particles, the angular dependence of the phase function is important. At small view angles, our approximation will underestimate the intensity and, at large view angles, it will overestimate the intensity. The reason for this is that the two-stream solutions take the energy in the narrow forward-scattering peak and spread it to larger angles. In Appendix A, we show that our technique is very accurate for calculating fluxes that are just angle-weighted integrals of the intensity over all angles. Thus, if the approximate solution underestimates intensity for some view angles, it will overestimate it at other view angles so

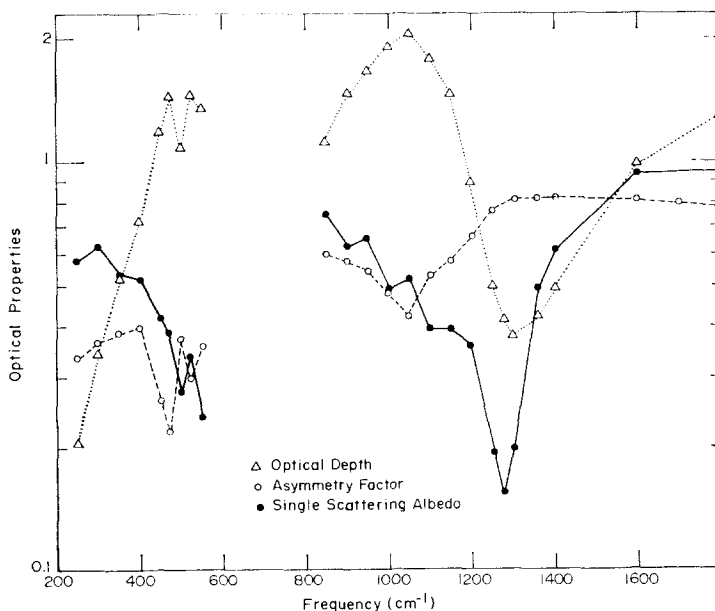


FIG. 2. The optical depth, single scattering albedo, and asymmetry factors for montmorillonite 219b; size distribution 1 (Fig. 5) and a visible optical depth of 1.5 were assumed.

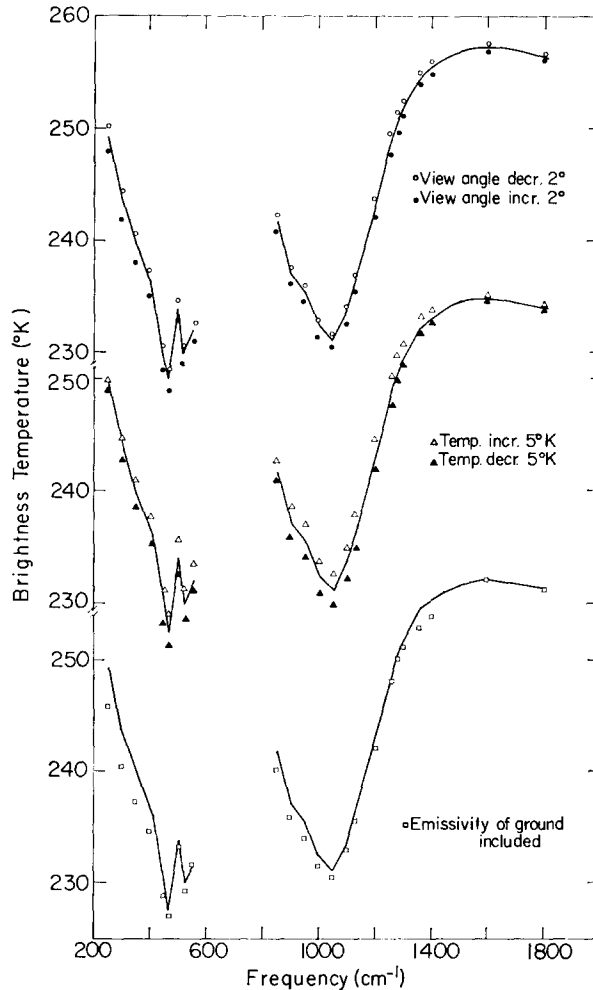


FIG. 3. Theoretical brightness temperature spectra. The solid curve is a standard case and the symbols show the changes due to an alteration of view angle, of ground emissivity, and of atmospheric temperature in the lowest two scale heights. As described in the text, the ground emissivity was calculated from an IRIS spectrum taken at the end of the 1971-1972 dust storm.

that the approximate integrated intensity nearly equals the exact integrated intensity.

Figure 1 illustrates the emergent intensity from a haze and a cloud calculated with our technique and with more sophisticated techniques (Liou, 1973; Yamamoto *et al.*, 1966). The approximation is quite satisfactory for the less forward-scattering haze calculation. It also does well for high and low optical depths in the cloud calculation. The apparent small error for large cloud optical depths (shown in Fig. 1)

may be due to a mistake by Yamamoto *et al.* since Liou (1973) gives results closer to our own. Our approximation does poorly for moderate cloud optical depths because the cloud particles are strongly forward scattering ($\bar{\cos\mu} = 0.86$). The error at $\arccos\mu \simeq 65^\circ$ is 8° in brightness temperature and the error of $\arccos\mu \simeq 15^\circ$ is 3° in brightness temperature, but in the opposite sense. While these errors are substantial, we consider our approximation to be adequate for the purposes of this paper.

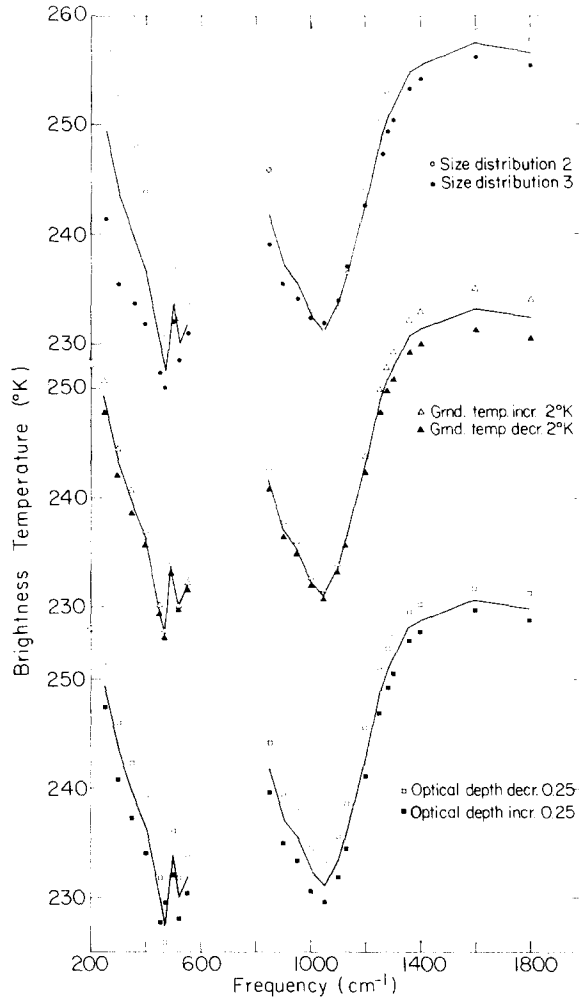


FIG. 4. Theoretical brightness temperature spectra. The solid curve is a standard case and the symbols show the changes due to an alteration of ground temperature, of optical depth, and of size distribution.

We have data sets from both large and small view angles and the errors in our approximation are of the opposite sign in these two cases. Therefore we make judgments based on comparisons with both data sets. Figure 2 illustrates typical optical properties used in our calculations. For $\nu < 1200 \text{ cm}^{-1}$, the optical properties are similar to those used in the haze calculation (Fig. 1) and our approximation should be sufficiently accurate. Between 1200 and 1350 cm^{-1} , $\cos\theta$ becomes large, but $\bar{\omega}_0$

and τ^* are small so the approximation should again be accurate. For $\nu > 1350 \text{ cm}^{-1}$, the optical properties do not favor our approximation and our results may be inaccurate. A final factor is that the standard deviation of the brightness temperature data is always at least 1°K and usually larger. In most cases, the error in our approximation will be less than the error in the data. Appendix A gives further examples of the accuracy of our approximate radiative transfer technique, which

show that the approximation is accurate for calculating fluxes over the whole range of possible optical properties.

INFORMATION CONTENT OF INFRARED AEROSOL SPECTRA

Radiative transfer calculations require that several input parameters be specified. The information content of a spectrum is determined by the ability to identify uniquely the role of each input parameter in generating the spectrum. If, for example, two input parameters had the same effect on the spectrum, we could not tell the value of either. On the other hand, we hope that input parameters of little interest, such as μ , do not have marked effects on the spectrum so that time does not have to be spent separating their effects from more interesting ones.

Figures 3 and 4 show the effects on the calculated spectrum of small changes in the input parameters. In each figure the solid line is a standard case that duplicates moderately well, but not exactly, the observed spectrum from the eighth orbit of the Mariner 9 spacecraft. The standard case uses size distribution 1 illustrated in Fig. 5, assumes a reference optical depth of 1.5, a ground temperature, T_g , of 265°K, a ground emissivity of unity, the optical constants of montmorillonite 219b, and the appropriate view angle and atmospheric temperature profile for Orbit 8.

The spectra averaged to produce the mean Orbit 8 spectrum had slightly different view angles. As shown in Fig. 3, a small change in the view angle does not markedly distort the spectrum, whereas changes of several degrees in the dust-cloud temperature in the lower atmosphere do begin to distort the spectrum. The brightness temperature at the band centers (near 500 and 1100 cm^{-1}) is more sensitive to the cloud temperature than is the brightness temperature in the band wings. The spectra averaged to produce the mean IRIS spectrum were taken from locations

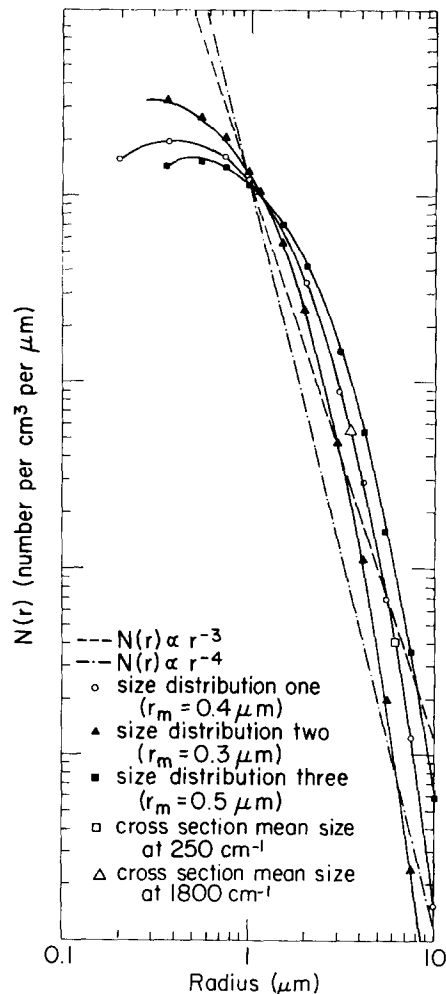


FIG. 5. Deirmendjian size distributions used in our study compared with power law size distributions. The Deirmendjian distributions all have $\alpha = 2$ and $\gamma = \frac{1}{2}$. Our calculations yield a cross-section weighted-mean particle size at each frequency. These sizes are indicated for two frequencies.

that probably had slightly different temperatures. However, differences between these spectra caused by different cloud temperatures could not have been significant because the standard deviation of the observed brightness temperature spectra at the band centers is less than the standard deviation in the band wings. It is more difficult to evaluate the reliability of the atmospheric temperature profiles

derived for us by the IRIS experimenters from analysis of the radiance in the 667-cm^{-1} CO_2 band. These atmospheric temperature profiles are uncertain because no dust absorption was taken into account in the derivation and, to a lesser extent, because there are uncertainties in the transmission coefficients of CO_2 and difficulties in inverting the radiance data to find the temperature profile. We believe this source of error is insignificant for our calculations because the effect shown in Fig. 3 for a 5° temperature change in the bottom 2 scale heights is not large, and because we did not detect any substantial changes in the difference between the observed and calculated spectrum as the dust cleared.

Another potential problem is the effect on the overall spectrum of the wavelength dependence of surface emission. The simplest way to account for this is to calculate the surface emissivity by assuming that the observed spectrum from a late orbit, in this case Orbit 206, is entirely due to emission from the surface. This is certainly an upper limit on the spectral contrast that might arise because of surface emission. Figure 3 shows that the overall spectrum is hardly influenced by the "upper-limit" surface emission spectrum. The dip near 1350 cm^{-1} in Fig. 3 results from CO_2 bands (Maguire, private communication) and the deviation below 400 cm^{-1} results from the numerous fine-scale gaseous absorption features below 400 cm^{-1} due to H_2O vapor, both of which depress the empirical spectrum used to derive the surface emissivity. The effect of ground emission is small because the ground temperature mainly determines the brightness temperature in the wings of the silicate bands; but in the wings the surface emissivity is very close to 1.

For these reasons, we have not considered either the view angle, the surface emission spectrum, or the atmospheric temperature profile to be free parameters. The view

angle is fixed by the observational data; the ground is assumed to be a perfect blackbody, and the IRIS-derived temperature-pressure profile is employed. We also assume that the dust was uniformly mixed in the atmosphere. Several investigations of the 1971–1972 dust storm (Leovy *et al.*, 1972; Conrath, 1975) suggest uniform mixing and our own conclusion (derived below) that the dust size distribution remained unchanged during the dust-storm dissipation justifies the assumption. Therefore the relation between optical depth and temperature is not considered a free parameter.

The optical depth at any wavelength can be found from the optical depth at another wavelength by a simple extinction cross-section scaling (Toon and Pollack, 1976). We have chosen $0.3\ \mu\text{m}$ as the wavelength to which τ^* is referenced. Therefore the only free parameters in our calculation are the total optical depth at this wavelength, τ^* , the ground temperature, T_g , the dust particle size distribution, $N(r)$, and the wavelength-dependent complex refractive index of the particles. The refractive index is fixed by the assumed particle composition.

Figure 4 illustrates the effect on the spectrum of changes in T_g and τ^* . Changes in τ^* are equivalent to changes in the number of particles in the dust cloud, and produce a shift of the spectrum which is nearly wavelength independent. Changing T_g has a greater effect at the wings of the bands than at the band centers. Because T_g and τ^* changes produce different effects on the spectrum, T_g and τ^* can be determined independently.

The size distributions we have explored here are modified gamma distributions as proposed by Deirmendjian (1969), which have the general form

$$N(r) = cr^\alpha \exp [-(\alpha/\gamma)(r/r_m)^\gamma],$$

where α and γ are adjustable constants and r_m is the mode radius. The normaliza-

tion constant c is not important because it is fixed by our choice of τ^* (Toon and Pollack, 1976). Many other $N(r)$ are used in the atmospheric aerosol literature (e.g., Toon and Pollack, 1976). However, over the range of particle sizes effective in producing the infrared spectra that we study, one cannot distinguish the other common $N(r)$ from the Deirmendjian functions. We have not investigated $N(r)$ that are multimodal. Uniform mixing requires that $N(r)$ be the same at all altitudes.

Figure 5 illustrates a standard size distribution function and two other Deirmendjian functions that differ only by their values of r_m . Figure 4 exhibits spectra calculated with these three size distributions. Increasing the relative numbers of large particles by increasing r_m broadens the bands and decreasing the number of large particles narrows the bands. If enough large particles are added, new bands will appear for materials such as quartz, and the band positions will shift to lower frequencies for other materials (Tuddenham and Lyon, 1960; Conel, 1969; Conrath *et al.*, 1973). The effects of changing $N(r)$ are more pronounced at low frequencies. The fact that the changes in the spectrum become larger as ν becomes smaller allows $N(r)$ changes to be distinguished from τ^* , or T_g changes which do not show systematic variations with ν . The spectrum is very sensitive to the size distribution and shows a systematic variation with ν because the single-particle extinction cross section is a strong function of the size parameter, $x = 2\pi\nu r$. When $x \ll 1$, the cross section is very small; when $x > 1$, the cross section is close to the particle geometric cross section. The IRIS spectra span an order of magnitude in ν so the extinction at one frequency relative to the extinction at another is very sensitive to the average cross-sectional area of those particles large enough to make $x \geq 1$ at each frequency. The size distribution inte-

grals used with the distribution functions in Fig. 5 to find the optical properties covered radii from about 0.1 μm to about 30 μm . However, the particles that contribute most to the extinction at 1800 cm^{-1} have $r \simeq 3 \mu\text{m}$ and the particles that contribute most to the extinction at 250 cm^{-1} have $r \simeq 6 \mu\text{m}$. Therefore we believe the IRIS spectra contain useful information about $N(r)$ from about 1 μm to about 10 μm radius. The reader should not overinterpret our conclusions about the size distribution. Since only particles between 1 and 10 μm are effective in creating the infrared spectra, we can only determine the slope of the size distribution between 1 and 10 μm . However, even though r_m is the parameter varied in our calculations, the spectra do not tell us the real mode radius, for it occurs at a size too small to interact efficiently with infrared radiation.

The final free parameter that enters the radiative transfer calculations is the dust composition which determines the refractive indices of the dust. We have used the refractive indices for quartz found by Spitzer and Kleinman (1961) and the values of basalt, andesite, obsidian, and basaltic glass found by Pollack *et al.* (1973). Additionally, we have determined

TABLE II
Chemical Composition of Montmorillonite and Granite (wt%)

	Granite	Montmorillonite 219b	Montmorillonite 222b
SiO ₂	71.30	63.20	53.10
Al ₂ O ₃	14.18	20.60	20.20
Fe ₂ O ₃	1.41	Total Fe as Fe ₂ O ₃	Total Fe as Fe ₂ O ₃
FeO	1.31	3.98	9.90
MgO	0.66	2.14	1.21
CaO	1.66	1.01	0.84
Na ₂ O	3.14	2.23	0.18
K ₂ O	5.29	0.26	1.16
H ₂ O ⁺	0.16	5.67	11.91
H ₂ O ⁻	0.10	Not measured	Not measured
CO ₂	0.23	Not measured	Not measured
TiO ₂	0.31	0.21	0.91
P ₂ O ₅	0.14	0.01	0.13
MnO	0.06	0.00	0.21
Total	99.95	99.31	99.75

TABLE III
 Refractive Indices of Montmorillonite and Granite

Frequency (cm^{-1})	Wavelength (μm)	Montmorillonite (219b)		Montmorillonite (222b)		Granite	
		n	k	n	k	n	k
250	40	2.18	0.14	2.18	0.16	2.43	0.05
260	38.5	2.18	0.15	2.17	0.19	2.43	0.06
270	37.0	2.18	0.15	2.18	0.17	2.49	0.07
280	35.7	2.19	0.12	2.24	0.21	2.53	0.08
290	34.5	2.25	0.15	2.23	0.26	2.59	0.09
300	33.3	2.25	0.15	2.22	0.28	2.63	0.11
310	32.3	2.31	0.19	2.22	0.27	2.73	0.16
320	31.3	2.31	0.21	2.27	0.33	2.74	0.31
330	30.3	2.35	0.31	2.24	0.41	2.67	0.36
340	29.4	2.27	0.35	2.16	0.42	2.69	0.23
350	28.6	2.23	0.24	2.13	0.34	2.93	0.23
360	27.8	2.37	0.27	2.20	0.34	3.29	0.31
370	27.0	2.38	0.43	2.20	0.32	3.15	1.34
380	26.3	2.27	0.33	2.27	0.33	2.76	1.23
390	25.6	2.38	0.44	2.33	0.37	2.37	0.71
400	25.0	2.29	0.30	2.40	0.39	2.64	0.55
410	24.4	2.50	0.30	2.50	0.51	2.83	0.74
420	23.8	2.63	0.37	2.51	0.63	2.85	0.95
430	23.3	2.80	0.54	2.53	0.72	2.72	1.13
440	22.7	2.90	0.83	2.58	0.87	2.53	1.25
450	22.2	2.93	1.14	2.64	1.10	2.40	1.22
460	21.7	2.72	1.70	2.45	1.58	2.30	1.25
470	21.3	1.92	1.92	1.81	1.71	2.20	1.29
480	20.8	1.45	1.55	1.45	1.35	2.07	1.29
490	20.4	1.45	1.07	1.46	0.99	1.91	1.29
500	20.0	1.68	0.85	1.68	0.80	1.54	1.24
510	19.6	1.94	1.03	1.91	0.98	1.63	0.75
520	19.2	1.75	1.42	1.80	1.33	1.91	0.78
530	18.9	1.39	1.38	1.46	1.40	1.82	1.05
540	18.5	1.18	1.21	1.22	1.26	1.52	0.97
550	18.2	1.11	1.02	1.12	1.08	1.53	0.61
560	17.9	1.04	0.89	1.06	0.96	1.73	0.49
570	17.5	1.06	0.72	1.02	0.85	1.93	0.60
580	17.2	1.05	0.64	0.98	0.73	1.95	0.78
590	17.0	1.09	0.52	1.00	0.59	1.82	0.91
600	16.7	1.13	0.47	1.05	0.52	1.55	0.94
610	16.4	1.14	0.41	1.07	0.47	1.39	0.74
620	16.1	1.14	0.35	1.08	0.42	1.46	0.45
630	15.9	1.19	0.25	1.09	0.36	1.60	0.47
640	15.6	1.27	0.18	1.14	0.27	1.58	0.51
650	15.4	1.35	0.21	1.19	0.25	1.54	0.41
660	15.2	1.36	0.20	1.22	0.22	1.58	0.31
670	14.9	1.39	0.15	1.25	0.20	1.67	0.28
680	14.7	1.46	0.18	1.29	0.14	1.73	0.27
690	14.5	1.46	0.19	1.37	0.18	1.78	0.27
700	14.3	1.46	0.17	1.37	0.19	1.82	0.31
710	14.1	1.48	0.12	1.37	0.18	1.82	0.34
720	13.9	1.55	0.15	1.38	0.16	1.81	0.33

TABLE III—(Continued)

Frequency (cm^{-1})	Wavelength (μm)	Montmorillonite (219b)		Montmorillonite (222b)		Granite	
		n	k	n	k	n	k
730	13.7	1.55	0.16	1.31	0.14	1.81	0.32
740	13.5	1.51	0.12	1.41	0.09	1.83	0.28
750	13.3	1.62	0.16	1.49	0.10	1.89	0.30
760	13.2	1.62	0.16	1.56	0.08	1.92	0.33
770	13.0	1.67	0.24	1.55	0.11	1.93	0.43
780	12.8	1.59	0.23	1.55	0.14	1.85	0.45
790	12.7	1.56	0.28	1.57	0.14	1.77	0.47
800	12.5	1.48	0.14	1.63	0.10	1.65	0.40
810	12.4	1.57	0.07	1.63	0.13	1.64	0.19
820	12.2	1.64	0.05	1.63	0.15	1.78	0.15
830	12.1	1.71	0.09	1.66	0.15	1.83	0.13
840	11.9	1.71	0.11	1.69	0.16	1.88	0.12
850	11.7	1.71	0.08	1.69	0.19	1.92	0.10
860	11.6	1.79	0.07	1.69	0.19	1.98	0.08
870	11.5	1.85	0.12	1.68	0.20	2.03	0.08
880	11.4	1.84	0.15	1.70	0.16	2.08	0.07
890	11.2	1.84	0.13	1.77	0.16	2.15	0.08
900	11.1	1.90	0.17	1.82	0.23	2.19	0.06
910	11.0	1.90	0.20	1.79	0.29	2.29	0.11
920	10.9	1.90	0.20	1.74	0.23	2.33	0.12
930	10.8	1.91	0.16	1.81	0.24	2.40	0.12
940	10.6	1.98	0.15	1.82	0.22	2.50	0.16
950	10.5	2.05	0.15	1.89	0.22	2.57	0.18
960	10.4	2.12	0.14	1.96	0.22	2.68	0.17
970	10.3	2.25	0.17	2.07	0.30	2.90	0.22
980	10.2	2.37	0.25	2.12	0.34	3.15	0.40
990	10.1	2.51	0.28	2.25	0.40	3.37	0.67
1000	10.0	2.78	0.59	2.40	0.66	3.46	1.25
1010	9.9	2.76	0.88	2.35	0.91	3.16	1.66
1020	9.8	2.69	1.24	2.28	1.11	2.89	1.84
1030	9.7	2.54	1.48	2.14	1.37	2.61	2.02
1040	9.6	2.32	1.80	1.92	1.56	2.30	2.08
1050	9.5	1.95	2.02	1.55	1.70	2.06	2.06
1060	9.4	1.39	2.06	1.19	1.62	1.95	2.05
1070	9.35	1.00	1.77	0.93	1.45	1.66	2.14
1080	9.26	0.86	1.44	0.78	1.22	1.40	2.02
1090	9.17	0.86	1.21	0.71	0.99	1.23	1.85
1100	9.09	0.92	1.07	0.74	0.79	1.19	1.71
1110	9.01	0.95	1.04	0.89	0.69	1.13	1.67
1120	8.93	0.91	1.03	0.98	0.76	1.00	1.63
1130	8.85	0.85	0.98	0.80	0.75	0.88	1.53
1140	8.77	0.77	0.91	0.70	0.64	0.75	1.38
1150	8.70	0.73	0.80	0.69	0.49	0.83	1.26
1160	8.62	0.74	0.70	0.72	0.37	0.73	1.25
1170	8.55	0.74	0.64	0.79	0.30	0.64	1.14
1180	8.48	0.71	0.59	0.79	0.23	0.58	1.01
1190	8.40	0.68	0.48	0.89	0.15	0.55	0.87
1200	8.33	0.72	0.37	0.97	0.14	0.56	0.75
1210	8.26	0.77	0.31	1.01	0.14	0.56	0.64

TABLE III—(Continued)

Frequency (cm^{-1})	Wavelength (μm)	Montmorillonite (219b)		Montmorillonite (222b)		Granite	
		n	k	n	k	n	k
1220	8.20	0.82	0.26	1.04	0.14	0.57	0.50
1230	8.13	0.86	0.23	1.07	0.12	0.64	0.35
1240	8.07	0.87	0.19	1.11	0.11	0.79	0.26
1250	8.00	0.95	0.16	1.12	0.09	0.88	0.16
1260	7.94	1.00	0.14	1.13	0.08	0.93	0.14
1280	7.81	1.05	0.11	1.15	0.06	1.00	0.11
1300	7.69	1.08	0.09	1.17	0.05	1.07	0.09
1320	7.58	1.11	0.07	1.19	0.05	1.12	0.07
1340	7.46	1.14	0.06	1.21	0.04	1.16	0.06
1360	7.35	1.17	0.05	1.22	0.04	1.20	0.05
1380	7.25	1.19	0.04	1.23	0.03	1.22	0.04
1400	7.14	1.20	0.04	1.25	0.03	1.24	0.04
1600	6.25	1.32	0.01	1.31	0.01	1.36	0.02
1800	5.56	1.37	0.008	1.32	0.007	1.42	0.008
2000	5.00	1.42	0.005	1.37	0.004	1.49	0.005

the infrared optical constants of two montmorillonite samples and one granite sample for this study. The details of our work on the optical constants of these materials are described by Toon (1975). The chemical makeup of the samples studied and the numerical values of the optical constants are given in Tables II and III. Note that optical constants are difficult to determine in the infrared and errors are wavelength-dependent. The real part of the refractive index n can be found accurately at all wavelengths; the greatest errors are $\approx 5\%$. The imaginary part K can be found accurately in the bands, but when $K < 0.1$, the errors may become as large as a factor of 2. For example, Toon (1975) shows that the Kramers-Kronig technique for finding refractive indices fails near 1300 cm^{-1} and predicts a K for montmorillonite 219b that is larger by about 30% than the value found from a dispersion technique. The Kramers-Kronig K yields a brightness temperature several degrees lower than that calculated from the dispersion K . The region near 1300 cm^{-1} is particularly difficult to study. Near 1300 cm^{-1} , $n \approx 1$, so absorption

dominates. However, since K is uncertain near 1300 cm^{-1} , the absorption cannot be calculated with great accuracy. The region near 1300 cm^{-1} is also confused by inaccuracies in our radiative transfer technique and by numerous CO_2 bands between 1300 and 1450 cm^{-1} (Maguire, private communication). For these reasons, we do not greatly emphasize our fit to the experimental data near 1300 cm^{-1} .

A fundamental problem with interpretation based upon the optical constants of rocks and minerals stems from the chemical variability of these materials. Most rock-forming minerals are solid solutions of two or more end members and their optical properties vary continuously over a range corresponding to the range of chemical composition; a fact widely used for mineralogical analysis. Rocks are even less well defined and a given rock type such as "andesite" may embrace many different mineralogic contents and textures. Therefore, it is not really useful to obtain highly accurate optical constants for any single rock. One must also take the variability into account when deciding what constitutes a fit to experimental data.

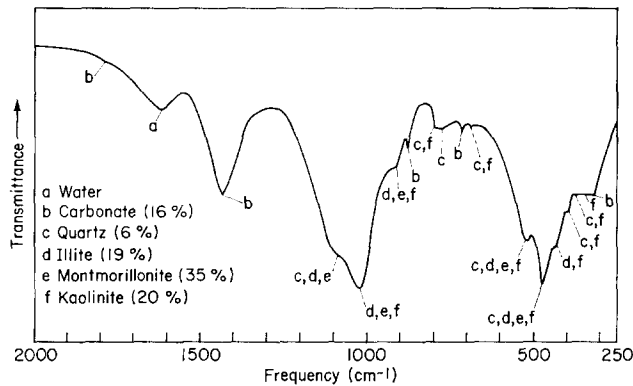


FIG. 6. An infrared spectrum of natural terrestrial dust, adapted from the work of Hoidale and Blanco (1969). The key identifies the composition of the dust by weight percent and identifies the spectral features.

Dust grains of the size composing Martian dust are smaller than the individual mineral grains that form many rocks. It is possible that the optical constants of a bulk rock will not simulate the optical behavior of the same rock dispersed. Glasses and minerals such as montmorillonite are fairly homogeneous. Laboratory spectra of inhomogeneous rocks such as granite seem similar to what one would expect using bulk measurements of optical constants. For example, the calculated spectra we show of granite, basalt, and montmorillonite are quite similar to the laboratory spectra published by Hunt *et al.* (1973), especially considering possible size distribution differences and the fact that our calculated spectra include emission from the dust.

The compositional information content of a spectrum depends on the similarities among the spectra of different classes of materials. For example, we have reproduced in Fig. 6 a typical infrared transmission spectrum of "natural" terrestrial dust suspended in a KBr pellet. This dust was filtered from the atmosphere over a desert basin in south-central New Mexico by Hoidale and Blanco (1969). They identified the major features in the spectrum and reported the dust to be about 35% by weight montmorillonite, 20% kaolinite,

and 19% illite, with small amounts of calcite (16%) and quartz (6%). For materials such as calcite with strong bands well removed from the silicate reststrahlen features at 1100 and 500 cm^{-1} , it is easy to derive mineralogical information from only a qualitative study. For silicates, however, a qualitative identification cannot easily be made because many of the bands overlap. It is well known (e.g., Hanel *et al.*, 1972b; Lyon, 1964) that the SiO_2 stretching mode near 1100 cm^{-1} is progressively shifted to lower frequencies as the SiO_2 content of igneous rocks decreases. By quantitatively taking $N(r)$ shifts of the band into account, it is possible to determine the approximate SiO_2 content, assuming that the rocks are igneous. The clay minerals have never been studied systematically to determine how SiO_2 content affects their band positions.

Hunt *et al.* (1973) have interpreted IRIS spectra by comparing the band positions in laboratory transmission spectra with the band positions in the IRIS spectra and by noting the remarkably smooth band profiles of the IRIS spectra. The IRIS spectra resolve numerous fine gaseous absorption features; they should resolve fine structure in the dust bands if such structure existed. Our calculations show that emission, absorption, and scattering in a size

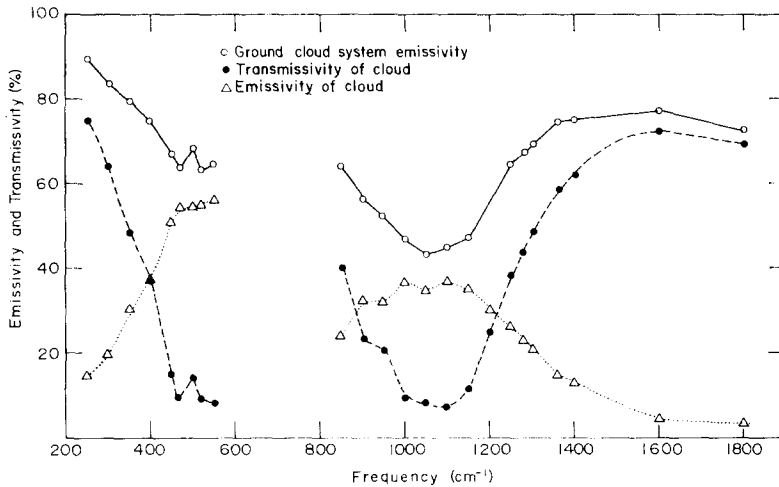


FIG. 7. The emissivity and transmissivity of a dust cloud calculated for the standard case. Also shown is the emissivity of the ground cloud system which includes both the light emitted by the dust cloud and the light emitted by the ground and transmitted through the cloud. All quantities are defined relative to the intensity of a blackbody at the ground temperature, $T' = 265^\circ\text{K}$.

distribution of dust does not destroy fine features in the emergent intensity spectra. The difficulty with the approach of Hunt *et al.* (1973), as they entirely anticipated, is that comparing a laboratory with a field spectrum never produces a positive identification. It is always possible that several materials may have their bands in the correct position and have fairly smooth bands. Moreover, a comparison of the spectra of Hoidale and Blanco (1969) (shown in Fig. 6) with those of Hunt *et al.* (1973) shows clearly that the spectrum of a mixture of materials has much less fine structure than the spectrum of any of the individual components. Since a mixture of minerals is very plausible geologically, one cannot exclude materials on the basis of the smoothness of their bands nor put any limits on the relative amounts of materials that have bands at fairly similar frequencies.

A factor not considered in our calculations is the shape of the dust particles. We have simply assumed the particles are spheres, and have employed Mie theory to calculate the optical properties of the

dust particles. Several experiments using particles with $x \approx 1$, K small, and moderate deviations from spherical shape have shown that Mie theory can be a good approximation for nonspherical particles (Greenberg *et al.*, 1971; Zerull and Giese, 1974). Calculations for very small ellipsoidal particles with high values of K show that Mie theory is a useful approximation if the particles are roughly equidimensional (Greenberg, 1972). Here we are interested in particles having $x \approx 1$, large K , and a distribution of sizes. Unfortunately, the effect of particle shape for these parameters has not been investigated. However, we believe that if the dust particles in the Martian dust storm were roughly equidimensional and not needles, for example, then Mie theory will be adequate for our calculations.

We have illustrated the importance of the free parameters for the emergent intensity spectrum and thereby determined that τ^* , T_g , $N(r)$, and composition can be found with varying degrees of precision. There is also much to be gained by examining the physical mechanisms that

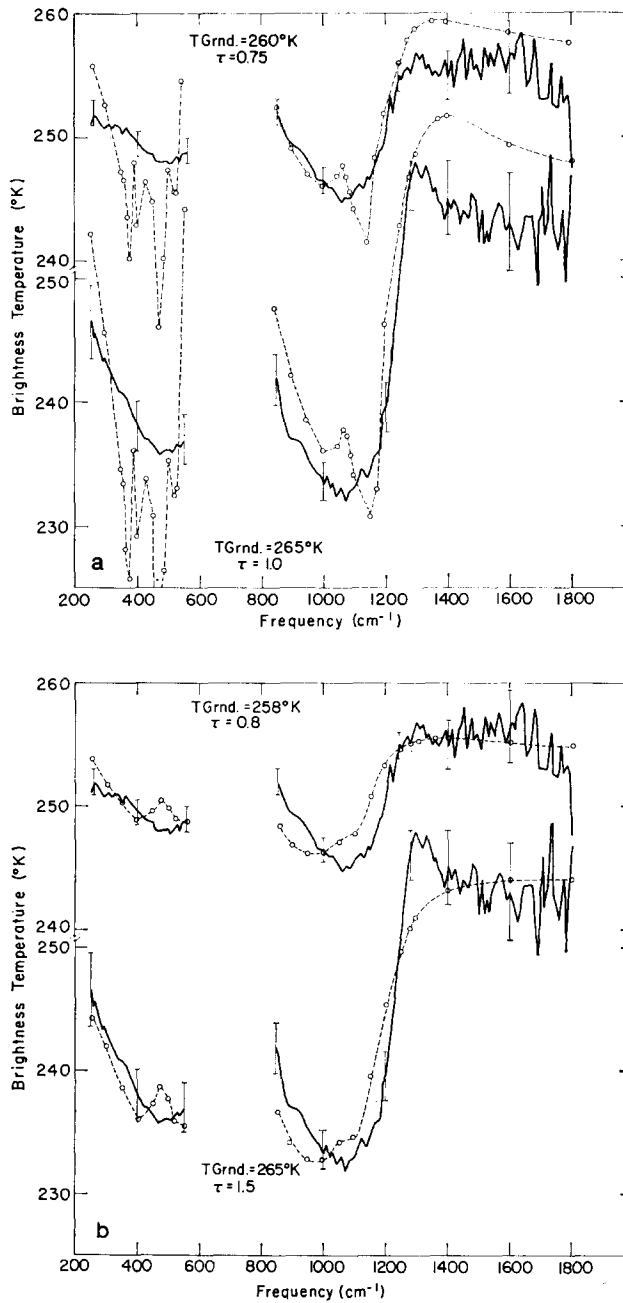


FIG. 8. Comparison of the IRIS spectra from Orbit 56 (top) and Orbit 8 (bottom) with calculations using the optical constants of (a) quartz, (b) basalt, (c) andesite, (d) basaltic glass, (e) obsidian, (f) granite, (g) montmorillonite 219b, and (h) montmorillonite 222b. All calculations employ size distribution 1 and the optical depth and temperature given in the figure. In Orbit 8, $\arccos\mu = 65.3^\circ$ while for Orbit 56 $\arccos\mu = 25.3^\circ$.

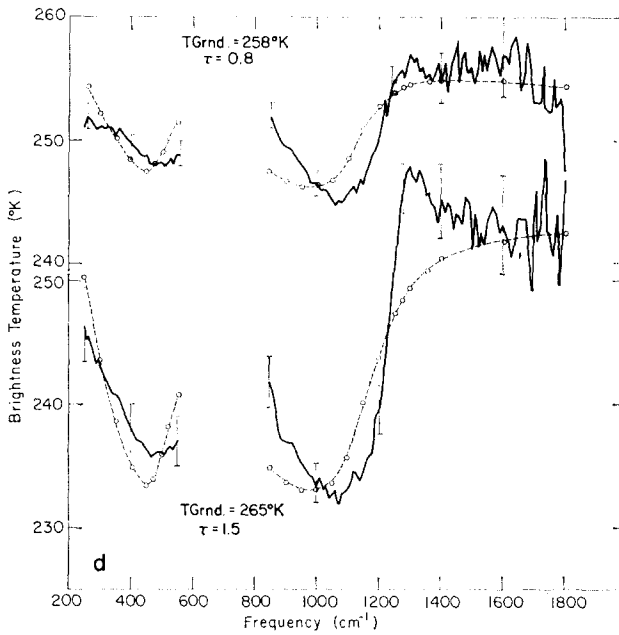
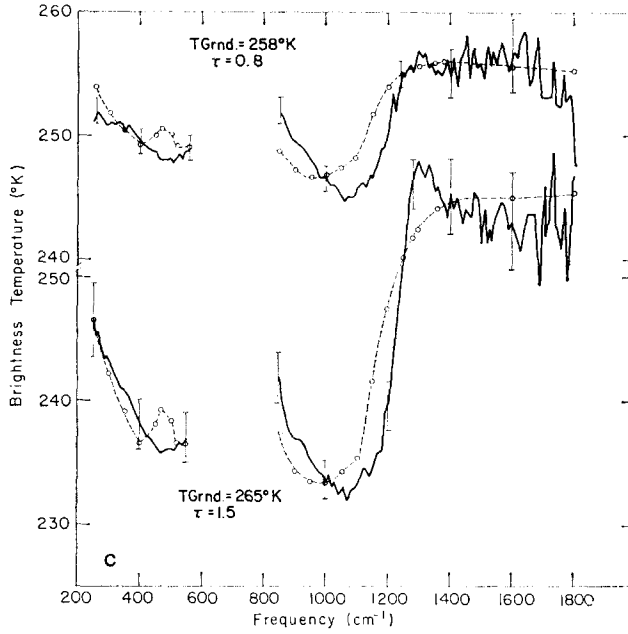


FIG. 8—Continued

give rise to the emergent intensity spectrum from a dust cloud such as the Martian one.

Figure 7 presents the emissivity and transmissivity of the dust cloud for our

standard case. Although the total emergent intensity, or ground-cloud system emissivity, looks superficially like the transmissivity, it is modified significantly by emission from the dust that fills in the

bottoms of the bands. The shape of the emission spectrum of the cloud is crudely the inverse of the shape of the $\bar{\omega}_0$ spectrum (Fig. 2), except in the region near 1280 cm^{-1} where the single scattering albedo has a

minimum that occurs because the real part of the refractive index is close to 1 and the imaginary part of the refractive index is small. This behavior would lead to an emission peak at the Christiansen

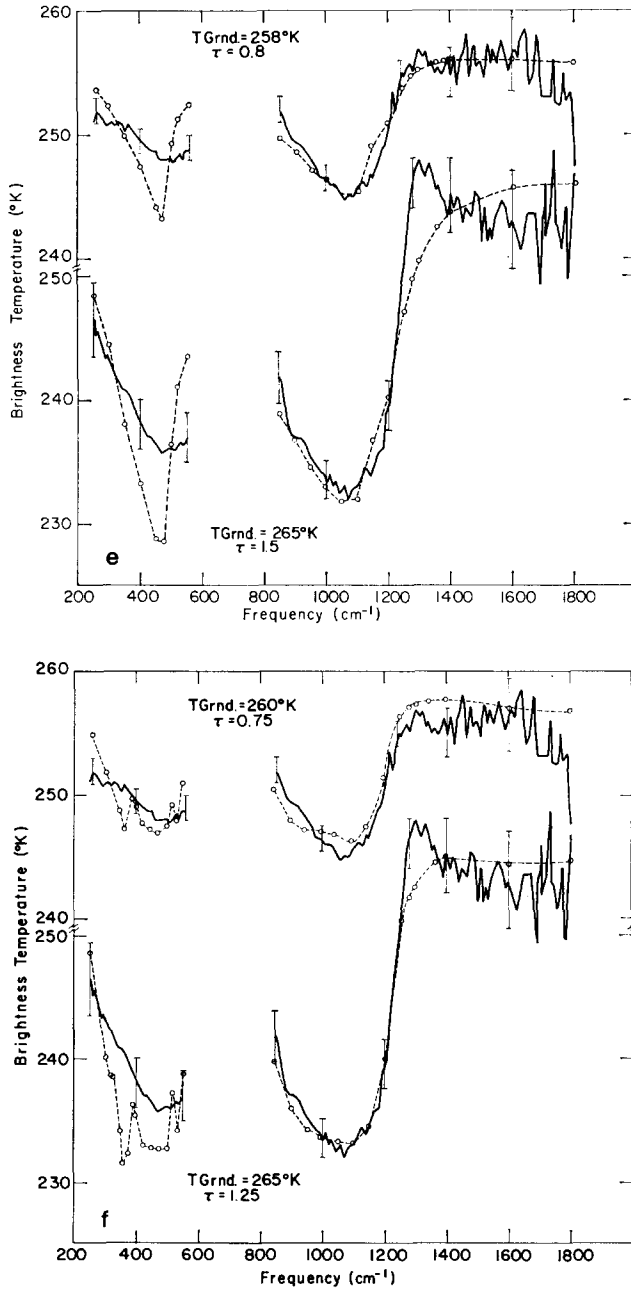


FIG. 8—Continued

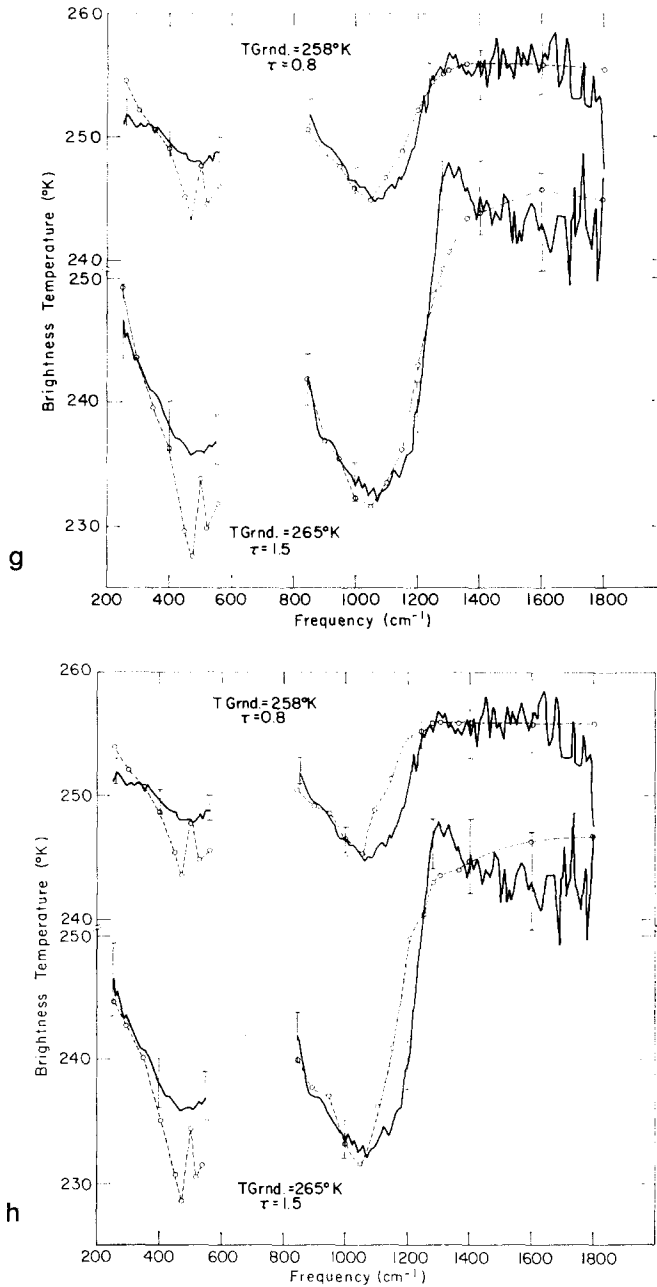


FIG. 8—Continued

frequency (here defined as the frequency where the real refractive index equals 1) in an optically thick emitting cloud (Hunt *et al.*, 1973). Figure 7 demonstrates that the transmission maximum occurs beyond

1400 cm⁻¹ and certainly is not near the 1280-cm⁻¹ Christiansen frequency.

Since the Christiansen frequency is a function of rock type, it has been valuable for compositional studies of optically thick

silicate powders (Logan *et al.*, 1973). Conel (1969) has shown that the transmission maximum of powders will occur at their Christiansen frequency if the particles are large enough. However, for quartz, Conel demonstrated that the frequency of the transmission maximum becomes shifted to frequencies higher than the Christiansen frequency when $r \lesssim 10 \mu\text{m}$. Physically, this happens because the transmission through an optically thin powder has a

maximum when the optical depth is minimum, which occurs close to the minimum in the extinction efficiency. For particles large compared to the wavelength, the extinction has a component due to scattering and so has a minimum where ω_0 is minimum, which is also where $n = 1$. For particles small compared to the wavelength, the extinction depends on the absorption and may therefore show no minimum near $n = 1$ since the absorption

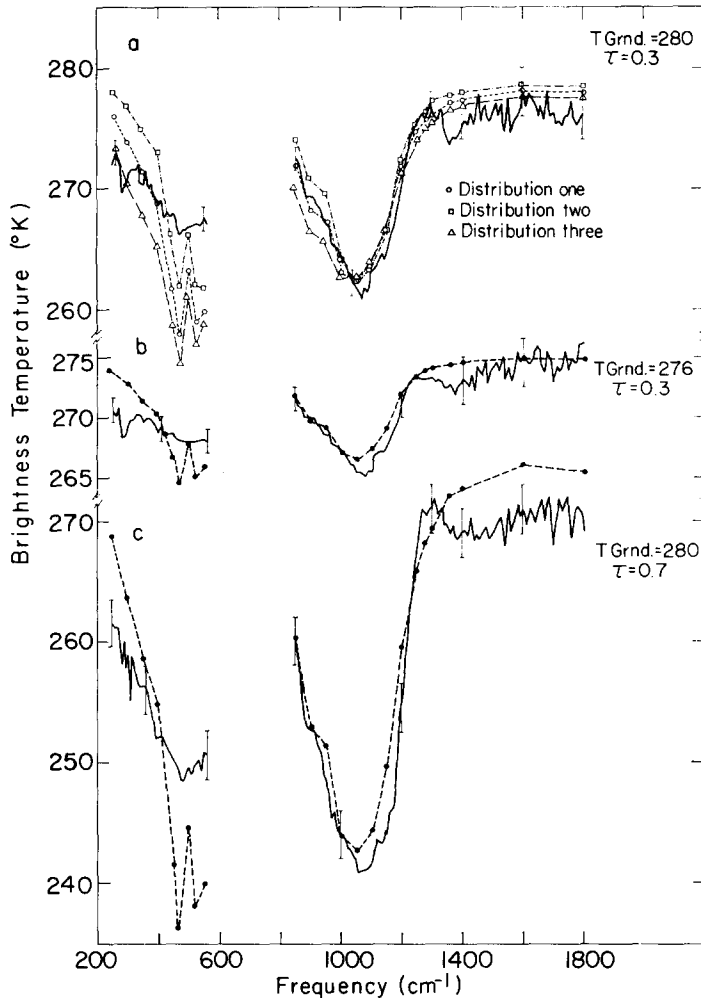


FIG. 9. Montmorillonite 219b computed spectra are compared to the observed spectra from Orbits 80 (c), 138 (b), and 154 (a). For Orbit 154, three size distributions are compared, but for the other orbits only size distribution 1 is used. Note that Fig. 4 compares all three distributions with parameters typical of Orbit 8, while Fig. 8g compares the Orbit 8 data with a size distribution 1 fit.

depends on K , not n . The effect can be seen experimentally for quartz in the work of Tuddenham and Lyon (1960). Our results confirm Conel's contention for materials other than quartz.

ANALYSIS OF IRIS SPECTRA

Figure 8 and 9 present IRIS spectra from a series of orbits spread through the early months of the Mariner 9 mission. The data are the solid curves with error bars and are graphed at approximately 10-cm^{-1} resolution, so many of the gaseous absorption bands below 480 and above 1300 cm^{-1} are not well resolved. The region from 550 to 850 cm^{-1} is occupied by an intense CO_2 absorption band which we have omitted for clarity. The diffuse bands centered near 1000 and 500 cm^{-1} are due to the suspended particles in the dust storm.

In Figs. 8 and 9, the dashed curves show our best fit to the IRIS spectra, using the optical constants of quartz, basalt, andesite, basaltic glass, obsidian, granite, and two samples of montmorillonite. None of these materials alone can account for the spectral features of the dust in the 1971–1972 dust storm. Quartz and granite have too much structure in their bands, and the low-frequency quartz bands are too strong. Andesite, basaltic glass, and basalt have both their bands at ν too low to fit the observed spectra. The 500-cm^{-1} band of obsidian is too sharp and too strong relative to the 1100-cm^{-1} band to fit the data. Both montmorillonite samples have too strong a band at 500 cm^{-1} ; both have a sharp double band at 500 cm^{-1} that does not appear in the IRIS data; montmorillonite 222b is too weak in the region between 1050 and 1200 cm^{-1} to fit the data. We have investigated a wide variety of changes in the free parameters, but have been unable to make a better fit to the IRIS spectra using these materials.

The number of rocks and minerals that can be studied is severely limited by the lack of optical constants. Perhaps some other single material can fit all the data. An important finding in our work is that the brightness temperature band centers near 1100 and 500 cm^{-1} occur very close to the frequency of maximum reflectivity for the polished slab. One can therefore turn to laboratory spectra (e.g., Lyon, 1964) and search for materials with smooth bands that peak at ~ 490 and $\sim 1090\text{ cm}^{-1}$, and in which the 490-cm^{-1} band is less developed than the 1090-cm^{-1} band. For example, rhyolite fits all these criteria, although its low-frequency band may fall short of 490 cm^{-1} .

One could probably discover other candidate materials by searching the literature for spectra or compiling spectra in the laboratory. This would not be a fruitful endeavor primarily because one could probably make mixtures of many materials whose spectra would then fit the data. For example, shales and sandstones, especially those composed mainly of clays and quartz (Hunt and Salisbury, 1975), would seem to be good candidates. Figure 10 exhibits the result of mixing montmorillonite and basalt. Basalt, andesite, anorthosite, and probably many plagioclase feldspars are obvious candidates to consider in a mixture because their bands at 500 cm^{-1} are weak and contain little structure, as noted by Hunt *et al.* (1973) and by Aronson and Emslie (1975). Indeed, the fit around 500 cm^{-1} (Fig. 10) is excellent. Figure 8 shows that basalt and andesite have their 1100-cm^{-1} bands at frequencies too low to explain the Mariner 9 observations. Aronson and Emslie (1975), whose analysis is considerably different from our own because it includes the effects of particle shape, reached the same conclusion for anorthosite and andesite. Figure 10, as well as the work of Aronson and Emslie, suggests that if basalt, andesite, or plagioclase feldspars are pre-

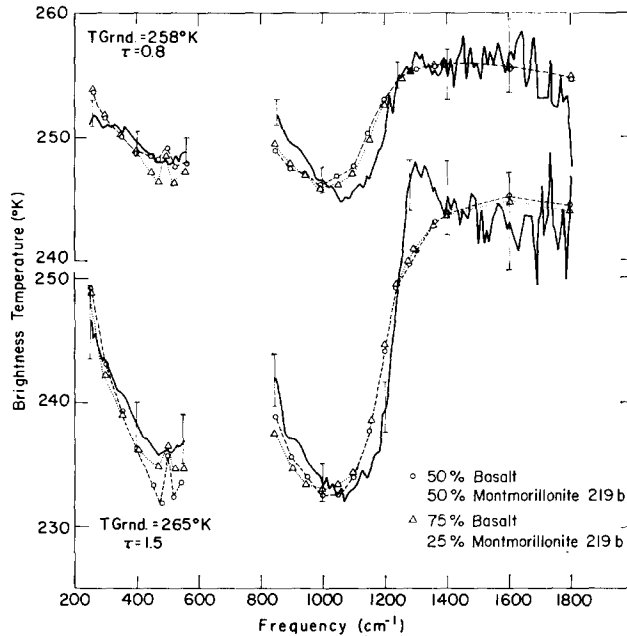


FIG. 10. Orbit 8 and 56 IRIS spectra are contrasted with spectra computed for a 50% basalt and montmorillonite 219b mixture (○) and for a 75% basalt, 25% montmorillonite 219b mixture (△).

sent, then the Mariner 9 data can be fitted only by having a substantial additional component of highly siliceous material.

Although we do not believe it is possible to determine the specific minerals composing the dust in the 1971–1972 storm, we do believe that some general compositional information can be obtained. Igneous rocks and minerals have their 1100-cm^{-1} bands shifted progressively to lower ν as their SiO_2 content decreases (Logan *et al.*, 1973). Our study includes granite and obsidian, which have SiO_2 contents of 71 and 76%, respectively. These rocks provide fairly good fits to the location of the 1100-cm^{-1} band whereas basalt, andesite, and basaltic glass with SiO_2 contents of 53 and 54%, respectively, provide poor fits. We did not study any igneous materials with SiO_2 contents near 60%, but their band positions should lie between those of the acidic and basic materials we did study. We agree with Hanel *et al.* (1972c) that the dust might be composed of an igneous rock with an

SiO_2 content between 60 and 70%. However, the IRIS data are most consistent with acidic rocks and therefore the SiO_2 content is probably greater than 65%. We do not agree with Hanel *et al.* that the average SiO_2 content could be as low as 50%, because the spectra of all basic rocks we studied clearly disagreed with the observed spectra. Hanel *et al.* adopted the 50% lower limit because they were only able to make qualitative comparisons. Although their comparison suggested about 60% or greater SiO_2 and was inconsistent with 50% SiO_2 , they felt that size distribution effects or other uncertainties in a qualitative comparison might allow 50% SiO_2 .

Although the band shift with SiO_2 content is well known for the igneous rocks, it has not been studied for weathering products such as clay minerals. We investigated two montmorillonite samples, one (219b) with about 63% SiO_2 and the other (222b), 53% SiO_2 by weight. Their maximum reflectivities were at the same

wavelength; only the values of the reflectivities differed. The Christiansen frequencies did shift with SiO_2 content, however. The SiO_2 content we estimated can be in error if clay minerals are significant constituents of the dust-storm particles. It would also be quite difficult to separate the clay minerals from a composite spectrum. Montmorillonite and illite are indistinguishable at 1100 cm^{-1} , and kaolinite (Hunt *et al.*, 1973) seems to have a fairly strong band near 900 cm^{-1} . There is in fact a weak shoulder in the IRIS data near 900 cm^{-1} and it is difficult to exclude kaolinite as a component of the cloud. On the other hand, this hardly amounts to a positive identification since many materials have bands in this region. The difficulty of separating the clay minerals in a composite spectrum can be judged from Hoidale and Blanco's work discussed earlier (Fig. 6).

We can place more restrictive limits on materials with bands that are at frequencies different from those of SiO_2 bands. Hunt *et al.* (1973) estimated that calcium carbonate could not compose even 10% of the dust. A glance at Hoidale and Blanco's spectrum in Fig. 6 confirms this limit. Spectra illustrated by Tuddenham and Stephens (1971) show that nitrates and borates could be only minor constituents of the dust. However, it would be difficult to put any limits on sulfates and phosphates that have bands near 1100 cm^{-1} and one could put only weak ($\ll 50\%$) limits on arsenates, vanadates, molybdates, and tungstates, all with bands near 900 cm^{-1} . The spectra of carbon-suboxide monomer and polymer (Smith *et al.*, 1963) demonstrate that carbon suboxides could at most be a very minor constituent of the dust.

The iron oxides have spectra that differ significantly from the IRIS spectra. Hematite (Adler *et al.*, 1950; Hunt *et al.*, 1973; Salisbury, private communication, 1974) has, in its pure form, no band near 1000

cm^{-1} , but it has a number of strong bands below 600 cm^{-1} . Adding hematite to a mixture of our previous candidate rocks and minerals will therefore produce a worse fit to the IRIS data by strengthening the low-frequency band relative to the high-frequency one. Hematite must be present only in small quantities, if at all. A spectrum of pure goethite has never been published. Adler *et al.* (1950) and Hunt *et al.* (1973) have published transmission spectra of SiO_2 -contaminated goethite. These spectra show bands below 600 cm^{-1} and a band at about 900 cm^{-1} . A reflection spectrum of a pressed pellet from this material (Salisbury, private communication, 1974) shows that the band at 900 cm^{-1} is weaker than the bands below 600 cm^{-1} , and that the bands below 600 cm^{-1} have about the same strength as those of montmorillonite. We conclude that there is no positive evidence for goethite, but it could form a significant fraction ($< 50\%$) of a mixture of materials. Hunt *et al.* (1973) have already pointed out that a thin ferric-oxide stain on the particles would have almost no effect on the spectrum. For example, montmorillonite 219b appears white to the eye, but montmorillonite 222b appears red. The difference between the amount of iron oxide in these two minerals (Table II) is only 6% and their infrared spectra differ very little (Fig. 8).

The particle size distribution plays an important role in determining the wavelength dependence of the emergent intensity. If the composition of the dust were known independently, it would be possible to obtain a detailed description of the size distribution from the infrared spectra. We have experimented with many different $N(r)$ combined with different τ^* and T_g but we have obtained the best results, for all materials investigated, using size distribution 1 shown in Fig. 5. Figures 4, 8, and 9 demonstrate that size distributions 2 and 3, also illustrated in Fig. 5, produce much poorer fits to the data at 1100 and

below 500 cm^{-1} than does size distribution 1. Because the results are so sensitive to $N(r)$, and because we obtained our best fits for all the materials with size distribution 1, we conclude that this distribution is close to the actual size distribution of particles in the dust storm. As pointed out earlier, the only significant information from the size distribution is its slope between about 1 and $10 \mu\text{m}$.

One very surprising discovery is that the size distribution that gives the best fit for the earliest orbits also gives the best fit to the latest orbits. Again we have tried many combinations of τ^* and T_g with the $N(r)$ trying to obtain good fits. In Fig. 4, we show that, for the conditions of Orbit 8, size distributions 2 and 3 give significantly different brightness temperature spectra than does size distribution 1. Figure 8g shows that size distribution 1 fits the data of Orbit 8 moderately well. In Fig. 9, we show attempts to fit montmorillonite to orbits spread from Orbit 80 to Orbit 154. Montmorillonite alone does not provide a perfect fit to the data. However, for all orbits the same distribution gives the best fit to the width of the 1000-cm^{-1} feature and to the opacity near 300 cm^{-1} . A size distribution such as size distribution 2 with fewer large particles provides a poorer fit, especially near 300 cm^{-1} , implying that the ratio of the number of particles of size $1 \mu\text{m}$ to those of about $10 \mu\text{m}$ remained approximately constant during the decay phase of the Martian dust storm.

Another parameter studied is the aerosol optical depth, τ^* . We have shown typical infrared values from our fit of montmorillonite to the Orbit 8 data in Fig. 2. For each orbit studied in Figs. 8 and 9, we also obtain an estimate of τ^* at $0.3 \mu\text{m}$, which we used as our reference wavelength. Figure 11 is a graph of our τ^* and those obtained by Pang and Hord (1973) using the Mariner 9 ultraviolet spectrometer. These results are not strictly com-

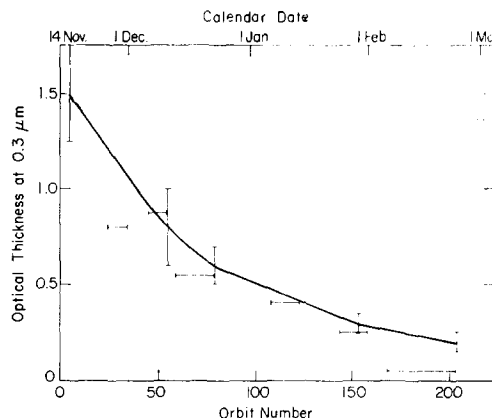


FIG. 11. Optical depth at $0.3 \mu\text{m}$, estimated from comparison of calculated spectra with the IRIS observed spectra, is given by the solid curve with vertical error bars. The horizontal error bars represent independent measurements by Pang and Hord (1973).

parable. Our measurements were made between -20 and -40° latitude and those of Pang and Hord were made over the Martian South Polar Cap at about -87° latitude. Also, it is not clear that we have chosen the correct optical properties for the rock in the visible, although the optical depth at 3000 \AA is not sensitive to the precise values of the optical constants. We believe our results substantiate the conclusions of Pang and Hord (1973) and Conrath (1975) that the dust storm clearing was fairly uniform in time. We have not analyzed enough orbits, however, to detect phenomena such as the mid-December resurgence noted by Hartmann and Price (1974). Since our optical depths seem rather close to those reported by Pang and Hord throughout the dust storm, our model of $N(r)$ for $r < 1 \mu\text{m}$ is probably reasonable. We conclude that the shape of the distribution between 0.1 and $5 \mu\text{m}$ did not undergo any drastic changes as the dust storm cleared. Our $N(r)$ for $r < 1 \mu\text{m}$ is rather similar to the few terrestrial dust size distributions that have been measured for $r < 1 \mu\text{m}$ (Gillette *et al.*, 1972). It is well known that the ratio of visible to

infrared optical depth is strongly controlled by the size distribution of the particles (e.g., Toon and Pollack, 1976). The fact that infrared optical depths were about as large as visible or uv optical depths during the dust storm limits the possible size distributions below $1 \mu\text{m}$; for example (Toon and Pollack, 1976), given the same refractive indices, τ^* at $\lambda = 0.3 \mu\text{m}$ would be 100 times larger than τ^* at $\lambda = 30 \mu\text{m}$ if the size distribution at all sizes were like the r^{-4} power law illustrated in Fig. 5. On the other hand, the r^{-3} power law shown in Fig. 5 will produce the same τ^* at 0.3 as at $30 \mu\text{m}$. Therefore the size distribution for $r < 1 \mu\text{m}$ must lie at or below the limit given by the r^{-3} distribution in Fig. 5. To decide which is the best $N(r)$ for $r < 1 \mu\text{m}$ would require knowledge of $\tau(\lambda)$ at $\lambda < 1 \mu\text{m}$. Our size distribution yields a mean particle radius weighted by cross section of about $3 \mu\text{m}$ at 3000 \AA , in fair agreement with the conclusion of Pang and Hord, but a factor of 3 larger than the near-infrared Mars 3 estimates of Moroz and Ksanfomaliti (1972) and a factor of 3 smaller than the crude estimate of Leovy *et al.* (1972) for the effective size at $0.588\text{-}\mu\text{m}$ wavelength. The mean particle size at 1800 cm^{-1} was also $3 \mu\text{m}$ and at 250 cm^{-1} the mean particle size was $6 \mu\text{m}$.

IMPLICATIONS FOR MARS

Our conclusions about the composition of the Martian dust can be put into perspective by comparison with the composition of terrestrial, meteorite, and lunar dust, by relating the dust composition to the surface composition of Mars, and by reconciling conclusions from infrared spectral data with conclusions from previous studies of the Martian surface in the visible and near infrared.

Many studies have been made of terrestrial windblown dust. Prospero and Bonatti (1969) captured soil particles over

the equatorial Pacific that were 40–50% SiO_2 . Junge (1963) quoted data showing that dust blown from the Sahara has 37–75% SiO_2 . The average terrestrial sediment has about 58% SiO_2 (Weast, 1966). Numerous mineralogical studies (Windom, 1969; Peterson, 1968; Delany *et al.*, 1967; Darby *et al.*, 1974; Prospero and Bonatti, 1969) have shown the importance of rock-forming silicates (quartz, feldspar, mica, amphibole), clays (montmorillonite, illite, kaolinite, chlorite), and carbonates in terrestrial windblown dust.

The lunar surface material has been examined in several studies. Apollo 16 highland rocks and soils had SiO_2 contents from 44 to 47% (Apollo 16 Preliminary Science Report, 1972). Similarly, glasses in the Apollo 11 mare soil samples had SiO_2 contents from 35 to 49%, although one glass sphere had 55% SiO_2 (Duke *et al.*, 1970). Lowman (1976) presents average SiO_2 contents for several mare and highland sites which range from 39 to 48% SiO_2 .

The SiO_2 content of meteorites varies with type: stony irons are 17 to 34% SiO_2 , carbonaceous chondrites are 23 to 33% SiO_2 , ordinary chondrites are 36 to 39% SiO_2 , and achondrites are 38 to 54% SiO_2 (Wood, 1963).

Our results for Mars indicate that the dust particles were not composed of igneous material with the SiO_2 content of meteorites, the lunar surface rocks, or lunar soil particles. On the other hand, the dust could have been igneous material with an SiO_2 content similar to or perhaps even higher than that of a typical terrestrial sediment, or the dust could have been composed of clay minerals similar to those that occur on the Earth. The important point is that the Martian dust has been differentiated by geologic or weathering processes.

Of course, it does not necessarily follow that the Martian crust needs to be chemically similar to the terrestrial crust.

Conrath *et al.* (1973) have argued that terrestrial sediments do not show significant SiO_2 differences from the crust, and that grain size fractionation might tend to make the SiO_2 content of dust lower, rather than higher, than the SiO_2 content of the rocks from which it arose. We add to this the above terrestrial observations showing that actual samples of windblown dust have about the same or perhaps slightly less SiO_2 than the average sediment. Likewise, on the Moon, there seems to be little difference between the rock and soil SiO_2 content. Such arguments by analogy are rather dangerous, however. The Earth's crust is so rich in SiO_2 , compared to the Moon or meteorites, that windblown dust would have to be nearly 100% quartz for gross fractionation to occur. Moreover, the weathering processes on the Moon must be much different from those on Mars. Mars has an atmosphere and, at least in the past, some water may have been present (e.g., Sagan *et al.*, 1973). Huguenin (1974) has suggested a weathering process on Mars that would create dust with a high SiO_2 content from rock with a lower SiO_2 content. Thus the high SiO_2 content of the Martian dust does not necessarily indicate that the crust as a whole has a high SiO_2 content. Likewise, if the dust is made of clay minerals, it does not necessarily indicate that the Martian crust is as siliceous as the Earth's.

Many studies of the Martian surface composition have been based on visible and near-infrared spectra of the Martian surface. Visible spectra implied some form of ferric oxide on Mars (e.g., Pollack and Sagan, 1967, 1969). Salisbury and Hunt (1969) have shown that visible spectra alone cannot be used to estimate the amount of ferric oxide; however, they believe near-infrared spectra of Mars limit the amount of limonite, goethite, or hematite to not more than a few percent. Unfortunately, the mid-infrared bands of iron oxides are overlapped by SiO_2 vibra-

tional bands, so we cannot put so restrictive a limit on the abundance of free iron oxides from the IRIS data.

Adams and McCord (1969) and Binder and Jones (1972) suggest that the bright and dark areas of the Martian surface are very similar mineralogically. They performed laboratory experiments showing that basalts coated with iron oxides could explain the visible and 1- μm features seen in Mars spectra. The visible and 1- μm features are due to transitions in iron oxides, and Salisbury and Hunt (1969) and Hunt *et al.* (1973) have emphasized that acidic igneous rocks containing iron oxides can also show the 1- μm spectral feature, and that the visible spectrum can be controlled by small amounts of weathering products such as iron oxides.

Recent spectra of Mars (McCord and Westphal, 1971; McCord *et al.*, 1971) show additional near-infrared bands between 1.4 and 2.2 μm . Sinton (1967) and Houck *et al.* (1973) have observed a strong infrared feature near 3 μm . All of these features are diagnostic of undissociated water molecules (Hunt and Salisbury, 1970). Hunt *et al.* (1974) show that these water bands do not occur in *unweathered* basic and ultrabasic rocks. The bands do occur, however, in weathering products such as clays, in acidic igneous rocks, and sometimes weakly in intermediate igneous rocks. The lack of such near-infrared features in basalt is one reason that Hunt *et al.* (1973) suggested that basalt could not be the dominant component of the Martian dust. However, both clays and acidic igneous rocks have these near-infrared bands so one cannot distinguish between them on the basis of the near-infrared spectrum.

Our conclusions from the IRIS spectra seem to be in accord with those of Hunt *et al.* (1973) based on the near-infrared spectrum of Mars. However, our results, which do exclude basalt as the exclusive dust-cloud component, cannot necessarily

be used to reject Adams and McCord's (1969) conclusion. It is possible that much of the dust in the Martian dust storm came from a restricted locale that is compositionally atypical, or that dust of a certain composition was preferentially lifted by the wind due to compositional changes with particle size. Indeed, some models of dust-storm generation (Sagan *et al.*, 1971; Gierasch and Goody, 1973) suggest that much of the dust comes from restricted locales such as the Hellas basin. The composition of material in the Hellas basin may not be typical of the Martian surface as a whole.

The dust size distribution also has implications for Mars. We have graphed two lines of Fig. 5 corresponding to $N(r) = r^{-\beta}$, one with $\beta \simeq 3$ and one with $\beta \simeq 4$. Although our Deirmendjian distributions have a varying slope, one can see that the slope is greater than 3. From 3 to 6 μm , the slope of size distribution 1 is rather close to 4. Size distribution 3 provides a much poorer fit to the IRIS data than size distribution 1, yet size distribution 3 is only slightly less steep than size distribution 1. Thus $N(r)$ with $\beta = 3$ would provide a poor fit indeed to the IRIS data. Several studies have been made of the particle size distribution for $r > 1 \mu\text{m}$ on Earth. Schütz and Jaenicke (1974) studied both the soil and aerosol size distribution in the Sahara and Gillette *et al.* (1972) made similar studies in rural Nebraska. Schütz and Jaenicke used a wet sieving technique so that any loose agglomerations in the aerosol or soil were broken up. For $1 \mu\text{m} \leq r \leq 10 \mu\text{m}$,

$$N(r) \propto r^{-\beta}$$

with $\beta \approx 3$. The soil $N(r)$ had a slope very similar to the aerosol value, but the soil $N(r)$ showed a relative maximum around 20–50 μm radius. Schütz and Jaenicke attributed the maximum in the soil size distribution near 30 μm to the redeposition of very large particles close

to the source. Small particles are carried large distances, thousands of kilometers. During a sandstorm Schütz and Jaenicke found that $N(r)$ had the same shape as the normal distribution, but had a larger number of particles of every size. Gillette *et al.* found the aerosol size distribution to be the same during periods when there was a vertical flux of aerosol in a dust storm as when there was not. Gillette *et al.* also studied the soil and aerosol size distribution below 1 μm , and they concluded that clay particles ($< 1 \mu\text{m}$) present in the soil clumped together to form larger aggregates in the aerosol because the wind-erosion mechanism was unable to disintegrate the agglomerates of soil particles. In a subsequent paper, Gillette *et al.* (1974) confirmed that the aerosol and soil distribution between $r = 1$ and 10 μm had a slope with $\beta \simeq 3$. However, by freeing the clay particles from the soil, they were able to produce a distribution with a steeper slope from 5 to 10 μm , although the slope became smaller from 1 to 5 μm .

Another significant set of $N(r)$ measurements was made by Gold *et al.* (1970) of the size distribution of lunar dust. They found a power law with $\beta \simeq 3$ for $1 \mu\text{m} < r < 10 \mu\text{m}$.

In addition to studies of $N(r)$ at the source regions, there have been studies farther from the source. Peterson (1968) examined the size distribution of dust at altitudes between 0.5 and 10 km over the Rajasthan Desert in northwest India, and found a power law between 1 and 10 μm with a slope of about 3.5. Delany *et al.* (1967) investigated wind-borne dust on the island of Barbados which they believed to have originated some 5000 km away in Europe and Africa. The size distribution was close to a power law and had a slope of about 4.5. Jaenicke (Schütz and Jaenicke, 1974; Junge, 1972) measured the size distribution of the Sahara dust about 1500 km from the African coast and found a size distribution from 1 to 10 μm that

was much steeper than one with a slope of $\beta = 3$.

A comparison of our results for the Martian dust-storm size distribution, $\beta \simeq 4$, with the foregoing results for the Earth and Moon leads us to three alternative hypotheses. First, the Martian dust-storm size distribution may be the same as the Martian soil distribution, which in turn is different from either the terrestrial or lunar size distribution by having relatively more 1- μm particles. That is, the Martian soil might be richer in clay-sized particles than either the Earth or the Moon. Alternately, Mars may have the same size distribution as the Earth but, as suggested by Sagan and Bagnold (1975), the cohesion between grains may be less. Thus the clay particles may not clump together, yielding a steeper aerosol size distribution in the manner suggested by Gillette *et al.* (1974). This would have great significance to the dust lifting process on Mars as suggested by Sagan and Bagnold (1976). The final alternative is that the soil size distributions are the same on the Earth, Moon, and Mars, and the aerosol size distribution just above the surface are the same on the Earth as on Mars. The steeper size distribution in the dust storm is then a consequence of taking the dust out of the surface boundary layer and transporting it vertically and horizontally over great distances. This is analogous to the terrestrial observation that the size distribution of Sahara dust blown thousands of kilometers over the Atlantic is much steeper than the size distribution just above the Sahara itself.

Major dust-source regions on Mars, and even local regions in which the wind carries away small particles, will be left with an excess of larger particles. On Earth, this effect produces an excess of particles of radius ~ 20 to $50 \mu\text{m}$ both in the Sahara and in the United States. It has long been suggested (e.g., Pollack and Sagan, 1967, 1969; Adams and McCord, 1969; but, for

a dissenting viewpoint see Moroz, 1976) that an excess of particles about this size would explain the difference between the bright and dark areas on Mars.

Martian dust storms are usually seen to develop in the same regions of Mars. If these regions continually supply all the dust that makes up the planet-wide dust storms as some, but not all, theories of dust-storm generation suggest (Sagan *et al.*, 1971; Gierasch and Goody, 1973), then weathering must continually replenish the dust particles smaller than about $50 \mu\text{m}$ or there must be a huge dust reservoir. Using the size distribution function, we calculate the total volume of aerosols in the 1971–1972 dust storm per square centimeter column of the atmosphere to be

$$V \simeq \tau_{\text{vis}} \times 1.7 \times 10^{-4} \text{ cm}^3 (\text{cm}^2 \text{ column})^{-1}.$$

(The number of particles $N \simeq \tau_{\text{vis}} \times 8 \times 10^6 \text{ cm}^{-2}$ column. This is less reliable because the size distribution below $1 \mu\text{m}$ is poorly known.) We now try to estimate an upper limit on the small-particle production rates. If $\tau \simeq 1$ and if we consider the dust to have been uniformly spread over the entire surface of Mars but to have originated from only the area of Hellas, then a volume of dust

$$\begin{aligned} V &\cong 1.7 \times 10^{-4} \frac{\text{cm}^3}{\text{cm}^2} \times \frac{4\pi \times 10^7 \text{ km}^2}{\pi \times 10^6 \text{ km}^2} \\ &= 6.8 \times 10^{-3} \frac{\text{cm}^3}{\text{cm}^2} \end{aligned}$$

is lost from the surface of the supply area. Since minor dust storms occurs every year on Mars and planetary obscuration about every 3 yr (Gierasch, 1974) a removal rate of $7 \times 10^{-3} \text{ cm yr}^{-1}$ must be an upper limit to the net erosion rate producing particles of $r \leq 50 \mu\text{m}$. There could be a substantial reservoir of dust in the source region created during some previous epoch. Such a reservoir would need to be rather large since, in 10^6 yr at

this upper-limit rate, approximately 70 m of dust would be removed. Dust of the size blown away in the storms constitutes much less than half the total soil judging from the Sahara data of Schütz and Jaenicke, making the required reservoir even larger. On the other hand, if this dust is continually replenished by erosion, it requires an erosion rate about two orders of magnitude below the lower limit of the eolian erosion rate predicted by Sagan (1973) of $\sim 6 \times 10^{1\pm 2}$ cm yr⁻¹ on a vertical wall. Of course, the wind erosion rate must also act to produce particles larger than 50 μ m and the source region may not have many vertical walls left. On the other hand, the removal rate is only a few times larger than the upper limit of the clay mineral formation rate predicted by Huguenin (1974). It is also possible that dust does not come from a restricted region of Mars, in which case no erosion rate can be calculated from the observations of the dust storm.

We concluded from the IRIS data that the size distribution of the dust from 1 to 10 μ m did not change appreciably during the dust-storm dissipation. Conrath (1975) used the Stokes-Cunningham equation to show that a free-falling, 10- μ m-radius particle in the Martian atmosphere will fall to the 5-mb pressure surface in less than 10 days. A 1- μ m-radius particle will take 10 times as long to fall out. Since the 10- μ m Stokes-Cunningham fall time is much less than the storm duration, the constant size distribution implies that Stokes-Cunningham fallout was not the dominant mechanism leading to the dust-storm clearing. From this observation, one can determine a lower limit to the atmospheric eddy viscosity. To keep a 10- μ m-radius particle suspended against fallout, the upward mixing rate must at least balance the downward fall rate. Crudely, the time to mix a particle through height, H , is $t = H^2/K_e$. A 10- μ m particle can fall to within a few scale heights of the surface

very rapidly; taking the fall time to equal the time to fall two scale heights yields $K_e \simeq (2 \times 10^6 \text{ cm})^2 / (5.6 \times 10^5 \text{ sec}) = 7 \times 10^6 \text{ cm}^2 \text{ sec}^{-1}$. This lower limit agrees well with the results of Conrath (1975), based on an independent method.

Several interesting conclusions follow from the result that Stokes-Cunningham fallout was not responsible for the particle removal. First, Conrath (1975) has pointed out that if Stokes-Cunningham fallout were important in the storm's dissipation, then the top of the atmosphere would have cleared much more rapidly than the lower part. Our results and those of Conrath suggest instead that the lower and upper atmospheres cleared at the same rate. Contrast would seem to improve faster in the lower atmosphere because removing half of a large number of particles has more effect on contrast than removing half of a smaller number of particles. Hartmann and Price (1974) have attempted to explain the observed contrast change by appealing to Stokes-Cunningham fallout in an atmosphere that contains much larger particles in its lower atmosphere. Having a size distribution that changes with altitude violates our uniform mixing assumption and seems unnecessary if Stokes-Cunningham fallout is not important. Our result that the size distribution did not change with time shows that particles are not removed by first falling to lower altitudes and then eventually to the surface. Rather, particles are continuously mixed in the atmosphere and are removed only when they are mixed into the surface boundary layer where they impact the surface or fall out. Another interesting problem arises if it is correct that the aerosol size distribution of the global dust storm differs from the near-surface size distribution. Then it will be necessary to consider boundary-layer processes that change the aerosol size distribution when the aerosol is injected out of the boundary layers into the main

atmosphere, but do not change the aerosol size distribution when the dust is slowly removed from the atmosphere and returned to the boundary layer and surface.

CONCLUSIONS

We have found that information on the composition, size distribution, and optical depth of the dust composing the Martian dust storm of 1971–1972 can be extracted from the IRIS spectra. The optical depth of the dust decreased uniformly during the dust-storm decay and infrared optical depths were comparable to those in the visible. The size distribution of the dust between 1 and 10 μm had a slope similar to that of terrestrial dust size distributions far from source regions. However, the dust size distribution was steeper than that of terrestrial or lunar soil samples or that of terrestrial dust in regions near a dust source. The cross-section weighted-mean particle radius of the dust ranged from 3 μm at 1800 cm^{-1} to 6 μm at 250 cm^{-1} . The dust size distribution did not change significantly during the decay of the dust storm, which implies that Stokes–Cunningham fallout of the dust was not an important dust-removal mechanism and that atmospheric eddy viscosities were at least of the order of $7 \times 10^6 \text{ cm}^2 \text{ sec}^{-1}$. Since Stokes–Cunningham fallout was not important, it is not necessary to invoke particle size variations with altitude to explain the temporal contrast changes observed in Mariner 9 television pictures. By terrestrial analogy, the Martian dust size distribution depleted small particles in the dust-source region, which could account for regional soil size distribution differences as have long been suggested by observations of the bright and dark regions on Mars. The dust-storm observations do not require that erosion currently produce new dust on Mars. However, predicted erosion rates are adequate to supply dust at the upper limit rate at which global dust

storms could remove dust from source regions. The composition of the dust was similar to that of terrestrial windblown dust, having an average SiO_2 content similar to acidic and intermediate igneous rocks, or perhaps clay minerals. The dust was probably a mixture of materials. Upper limits are set by the IRIS spectra of a few percent carbon suboxide or hematite and several tens of percent goethite. The dust mixture was not dominated by basic igneous rocks, but could have contained substantial quantities of basic igneous rock. The dust composition was therefore clearly different from the composition of lunar soil and dust or the composition of meteorites. Since the dust is not dominated by basic rock, geochemical differentiation or weathering is important on Mars. The Martian dust, in contrast to terrestrial dust, contained a few percent carbonate at most. Because the composition of the dust is not necessarily identical to the composition of the surface as a whole, our compositional results do not contradict other studies that have suggested the Martian crust is composed mainly of basalt.

APPENDIX A

The monochromatic equation of radiative transfer in a homogeneous plane-parallel atmosphere with the positive direction outward from the surface and an optical depth of zero at the top is

$$\mu \frac{dI_\nu(\tau_\nu, \mu, \theta)}{d\tau_\nu} = I_\nu(\tau_\nu, \mu, \theta) - S_\nu(\tau_\nu, \mu, \theta).$$

In the two-stream approximation with an emitting, scattering aerosol but no gaseous emission or absorption, the equation becomes

$$\begin{aligned} (1/3^{1/2})dI_+/d\tau &= I_+ - S_+, \\ -(1/3^{1/2})dI_-/d\tau &= I_- - S_-, \end{aligned}$$

where

$$\begin{aligned} S_+ &= \frac{1}{2}\bar{\omega}_0(1 + \text{cosbar})I_+ \\ &+ \frac{1}{2}\bar{\omega}_0(1 - \text{cosbar})I_- \\ &+ (1 - \bar{\omega}_0)B(\tau), \end{aligned}$$

$$S_- = \frac{1}{2}\bar{\omega}_0(1 + \text{cosbar})I_- + \frac{1}{2}\bar{\omega}_0(1 - \text{cosbar})I_+ + (1 - \bar{\omega}_0)B(\tau).$$

In this equation, $\bar{\omega}_0$, the single scattering albedo, is

$$\bar{\omega}_0 = \int_{\Omega} P(\cos \Theta)d\Omega/4\pi$$

and cosbar , the asymmetry factor, is

$$\text{cosbar} = (1/\bar{\omega}_0) \int_{\Omega} \cos \Theta P(\cos \Theta)d\Omega/4\pi.$$

In these equations, $P(\cos \Theta)$ is the scattering phase function and Θ is the angle between the incident and scattered wave normals with the origin of the coordinates at the scattering center.

The solution to these equations is subject to boundary conditions

$$I_- = 0 \quad (\tau = 0), \\ I_+ = \epsilon B^* \quad (\tau = \tau^*).$$

Here ϵ is the ground emissivity and B^* is the Planck function evaluated at the ground temperature. The surface reflectivity is assumed to be zero. The solution is

$$I_+ = \Gamma(K + V_1)e^{\lambda\tau} + \Gamma^{-1}(V_2 - \alpha - K)e^{-\lambda\tau}, \\ I_- = (K + V_1)e^{\lambda\tau} + (V_2 - \alpha - K)e^{-\lambda\tau},$$

where

$$\Gamma = \frac{\lambda + 3^{1/2}(1 - \bar{\omega}_0)}{\lambda - 3^{1/2}(1 - \bar{\omega}_0)}, \\ \lambda = [3(1 - \bar{\omega}_0)(1 - \bar{\omega}_0 \text{cosbar})]^{1/2},$$

$$K = \frac{\epsilon B^* + (\alpha/\Gamma)e^{-\lambda\tau^*}}{\Gamma e^{\lambda\tau^*} - (e^{-\lambda\tau^*}/\Gamma)},$$

$$V_1(\tau) = \frac{3^{1/2}(1 - \bar{\omega}_0)}{(1 - \Gamma)} \int_{\tau^*}^{\tau} dt e^{-\lambda t} B(t),$$

$$V_2(\tau) = \frac{3^{1/2}(1 - \bar{\omega}_0)\Gamma}{(\Gamma - 1)} \int_{\tau^*}^{\tau} dt e^{\lambda t} B(t),$$

and

$$\alpha = V_1(0) + V_2(0).$$

The formal solution to the equation of transfer for the emergent intensity is

$$I(0, +\mu) = \epsilon B^* e^{-\tau^*/\mu} + \int_0^{\tau^*} e^{-t/\mu} S(t) dt/\mu.$$

We use the two-stream source function $S_+(t)$ as an approximation to $S(t)$. After some manipulation, we find that

$$S_+ = (1 - \omega_0)B(t) + (bd/2)e^{\lambda t} \int_t^{\tau^*} e^{-\lambda\tau} B(\tau) d\tau + (ac/2)e^{-\lambda t} \int_0^t e^{\lambda\tau} B(\tau) d\tau + \left[\epsilon B^* - e^{-\lambda\tau^*}(c/2) \int_0^{\tau^*} d\tau e^{\lambda\tau} B(\tau) \right] \times [(db^2 e^{\lambda t} - ac^2 e^{-\lambda t})/f] + (c^2 d/2) \int_0^{\tau^*} d\tau e^{-\lambda\tau} B(\tau) \times [(be^{\lambda t} e^{-\lambda\tau^*} - ae^{-\lambda t} e^{+\lambda\tau^*})/f],$$

where

$$a = 1 + \lambda/3^{1/2}, \\ b = 1 - \lambda/3^{1/2}, \\ c = \lambda - 3^{1/2}(1 - \bar{\omega}_0), \\ d = \lambda + 3^{1/2}(1 - \bar{\omega}_0), \\ f = d^2 e^{\lambda\tau^*} - c^2 e^{-\lambda\tau^*}, \\ \lambda = [3(1 - \bar{\omega}_0)(1 - \bar{\omega}_0 \text{cosbar})]^{1/2}.$$

Although this solution may appear lengthy, it is in fact computationally very fast and well behaved. The solution for the emergent intensity is analytic when the temperature of the cloud is constant and when $\bar{\omega}_0 = 1$. When $\bar{\omega}_0 = 1$, the source function goes to the limit

$$S_+ = \epsilon B^* \times \left[\frac{6\tau(1 - \text{cosbar}) + 2(3)^{1/2}(1 + \text{cosbar})}{6\tau^*(1 - \text{cosbar}) + 4(3)^{1/2}} \right].$$

TABLE IV
Flux Comparisons between Approximate Technique and Exact Solutions

$\bar{\omega}_0 = 1, \text{cosbar} = 0$ (Sagan and Pollack, 1967)				
τ^*	Transmission exact		Transmission approximate	
0.05	0.955		0.9548	
0.1	0.916		0.9160	
0.15	0.881		0.8814	
0.25	0.820		0.8215	
0.50	0.704		0.7067	
1.00	0.552		0.5563	
$\bar{\omega}_0 = 1, \tau^* = 20$ (Sagan and Pollack, 1967)				
Cosbar	Transmission exact		Transmission approximate	
0.0	0.062		0.0588	
0.7	0.179		0.1651	
0.9	0.388		0.3689	
1.0	1.0		1.0000	
$\bar{\omega}_0 = 0.3637, \text{cosbar} = 0.8487$ (Hunt, 1973)				
τ^*	Exact values		Approximate values	
	Transmissivity	Emissivity	Transmissivity	Emissivity
0.1	0.8803	0.1129	0.8856	0.1099
0.5	0.5669	0.4205	0.5786	0.4077
1	0.3442	0.6405	0.3508	0.6313
2	0.1370	0.8471	0.1299	0.8503
5	0.01062	0.9735	0.0061	0.9738
$\bar{\omega}_0 = 0.52447, \text{cosbar} = 0.93112$				
τ^*	Exact values		Approximate values	
	Transmissivity	Emissivity	Transmissivity	Emissivity
0.1	0.9084	0.08657	0.9137	0.0833
0.5	0.6486	0.3405	0.6641	0.3257
1	0.4429	0.5440	0.4533	0.5324
2	0.2188	0.7677	0.2090	0.7739
5	0.0315	0.9542	0.0184	0.9638

We pointed out in the text that the solution is exact in the limit $\bar{\omega}_0 = 0$ and discussed errors in finding brightness temperatures. In Table IV, we show a number of comparisons of fluxes calculated with a six-point quadrature integral of the emergent intensity multiplied by the cosine of the emergent angle. Generally, the trans-

missivity are within 1% in absolute value of the more accurate results.

ACKNOWLEDGMENTS

We thank Dr. J. Salisbury for measuring the reflection spectrum of montmorillonite and for several useful comments. We are also grateful to the IRIS experimenters, particularly Drs. R. Hanel,

V. Kunde, J. Pearl, and R. Curran, for their careful selection of the data used in our study and for several helpful suggestions. We benefited from discussions with Drs. J. Veverka and J. Cuzzi and were assisted by Ms. A. Summers and B. Baldwin in programming. This work was supported in part by the Planetary Office, NASA, under Grant NGR 33-010-220 and by Atmospheric Sciences Section, NSF, under Grant ATM 74-20458 A01 both to Cornell University; during part of the study, O. Toon was supported by a National Academy of Sciences Resident Research Associateship at Ames Research Center.

REFERENCES

- ADAMS, J. B., AND MCCORD, T. B. (1969). Mars: Interpretation of spectral reflectivity of light and dark regions. *J. Geophys. Res.* **74**, 4851-4856.
- ADLER, H. H., KERR, P. F., BRAY, T. T., STEVENS, N. P., HUNT, J. M., KELLER, W. D., AND PICKETT, E. E. (1950). Infrared spectra of reference clay minerals. Columbia University, available from DDC under AD 825096.
- APOLLO 16 Preliminary Science Report (1972). NASA SP-315.
- ARONSON, J. R., AND EMSLIE, A. G. (1975). Composition of the Martian dust as derived by infrared spectroscopy from Mariner 9. *J. Geophys. Res.* **80**, 4925-4931.
- BINDER, A. B., AND JONES, J. C. (1972). Spectrophotometric studies of the photometric function, composition, and distribution of the surface materials of Mars. *J. Geophys. Res.* **77**, 3005-3020.
- CHANDRASEKHAR, S. (1960). *Radiative Transfer*. Dover, New York.
- CONEL, J. E. (1969). Infrared emissivities of silicates: Experimental results and a cloudy atmosphere model of spectral emission from condensed particulate mediums. *J. Geophys. Res.* **74**, 1614-1634.
- CONRATH, B. (1975). Thermal structure of the Martian atmosphere during the dissipation of the dust storm of 1971. *Icarus* **24**, 36-46.
- CONRATH, B., CURRAN, R., HANEL, R., KUNDE, V., MAGUIRE, W., PEARL, J., PIRRAGLIA, J., WELKER, J., AND BURKE, T. (1973). Atmospheric and surface properties of Mars obtained by infrared spectroscopy on Mariner 9. *J. Geophys. Res.* **78**, 4267-4278.
- CURRAN, R. J., CONRATH, B. J., HANEL, R. A., KUNDE, V. G., AND PEARL, J. C. (1973). Mars: Mariner 9 spectroscopic evidence for H₂O ice clouds. *Science* **182**, 381-383.
- DARBY, D. A., BURCKLE, L. H., AND CLARK, D. L. (1974). Airborne dust on the Arctic pack ice, its composition and fallout rate. *Earth Planet. Sci. Lett.* **24**, 166-172.
- DEIRMENDJIAN, D. (1969). *Electromagnetic Scattering of Spherical Polydispersions*. Elsevier, New York.
- DELANY, A. C., DELANY, A. C., PARKIN, D. W., GRIFFIN, J. J., GOLDBERG, E. D., AND REIMANN, B. E. F. (1967). Airborne dust collected at Barbados. *Geochim. Cosmochim. Acta* **31**, 885-909.
- DUKE, M. B., WOO, C. C., BIRD, M. L., SELLERS, G. A., AND FINKELMAN, R. B. (1970). Lunar soil: Size distribution and mineralogical constituents. *Science* **167**, 648-650.
- GIERASCH, P. J. (1974). Martian dust storms. *Rev. Geophys. Space Phys.* **12**, 730-734.
- GIERASCH, P. J., AND GOODY, R. M. (1973). A model of a Martian great dust storm. *J. Atmos. Sci.* **30**, 169-179.
- GILLETTE, D. A., BLIFFORD, I. H., JR., AND FENSTER, C. R. (1972). Measurements of aerosol size distributions and vertical fluxes of aerosols on land subject to wind erosion. *J. Appl. Meteorol.* **11**, 977-987.
- GILLETTE, D. A., BLIFFORD, I. H., AND FRYREAR, D. W. (1974). The influence of wind velocity on the size distributions of aerosols generated by the wind erosion of soils. *J. Geophys. Res.* **79**, 4068-4075.
- GOLD, T., CAMPBELL, M. J., AND O'LEARY, B. T. (1970). Optical and high-frequency electrical properties of the lunar sample. *Science* **167**, 707-709.
- GREENBERG, J. M. (1972). Absorption and emission by nonspherical particles. *J. Colloid Interface Sci.* **39**, 513-519.
- GREENBERG, J. M., WANG, R. T., AND BANGS, L. (1971). Extinction by rough particles and the use of Mie theory. *Nature Phys. Sci.* **230**, 110-112.
- HANEL, R. A., SCHLACHMAN, B., BREIHAN, E., BYWATERS, R., CHAPMAN, F., RHODES, M., RODGERS, D., AND VANOUS, D. (1972a). The Mariner 9 Michelson interferometer. *Appl. Opt.* **11**, 2625-2634.
- HANEL, R. A., CONRATH, B. J., HOVIS, W. A., KUNDE, V. G., LOWMAN, P. D., PEARL, J. C., PRABHAKARA, C., SCHLACHMAN, B., AND LEVIN, G. V. (1972b). Infrared spectroscopy experiment on the Mariner 9 mission: Preliminary results. *Science* **175**, 305-308.
- HANEL, R., CONRATH, B., HOVIS, W., KUNDE, V., LOWMAN, P., MAGUIRE, W., PEARL, J., PIRRAGLIA, J., PRABHAKARA, C., SCHLACHMAN, B., LEVIN, G., STRAAT, P., AND BURKE, T. (1972c). Investigation of the Martian environment by infrared spectroscopy on Mariner 9. *Icarus* **17**, 423-442.

- HARTMANN, W. K., AND PRICE, M. J. (1974). Mars: Clearing of the 1971 dust storm. *Icarus* 21, 28-34.
- HOIDALE, G. B., AND BLANCO, A. J. (1969). Infrared absorption spectra of atmospheric dust over an interior desert basin. *Pure Appl. Geophys.* 74, 151-164.
- HOUCK, J., POLLACK, J. B., SAGAN, C., SHAACK, D., AND DECKER, J. (1973). High altitude aircraft infrared spectroscopic evidence for bound water on Mars. *Icarus* 18, 470-480.
- HUGUENIN, R. L. (1974). The formation of goethite and hydrated clay minerals on Mars. *J. Geophys. Res.* 79, 3895-3905.
- HUNT, G. E. (1973). Radiative properties of terrestrial clouds at visible and infra-red thermal window wavelengths. *Quart. J. Roy. Met. Soc.* 99, 346-369.
- HUNT, G. R., LOGAN, L. M., AND SALISBURY, J. W. (1973). Mars: Components of infrared spectra and the composition of the dust cloud. *Icarus* 18, 459-469.
- HUNT, G. R., AND SALISBURY, J. W. (1970). Visible and near-infrared spectra of minerals and rocks: I. Silicate minerals. *Mod. Geol.* 1, 283-300.
- HUNT, G. R., AND SALISBURY, J. W. (1975). Mid-infrared spectral behavior of sedimentary rocks. AFCRL Report TR-75-0356.
- HUNT, G. R., SALISBURY, J. W., AND LENHOFF, C. J. (1974). Visible and near infrared spectra of minerals and rocks: IX. Basic and ultrabasic igneous rocks. *Mod. Geol.* 5, 15-22.
- JUNGE, C. E. (1963). *Air Chemistry and Radioactivity*. Academic Press, New York.
- JUNGE, C. E. (1972). Our knowledge of the physico-chemistry of aerosols in the undisturbed marine environment. *J. Geophys. Res.* 77, 5183-5200.
- LEOVY, C. B., BRIGGS, G. A., YOUNG, A. T., SMITH, B. A., POLLACK, J. B., SHIPLEY, E. N., AND WILDEY, R. L. (1972). The Martian atmosphere: Mariner 9 television experiment progress report. *Icarus* 17, 373-393.
- LIU, K. (1973). A numerical experiment on Chandrasekhar's discrete-ordinate method for radiative transfer: Applications to cloudy and hazy atmospheres. *J. Atmos. Sci.* 30, 1303-1326.
- LOGAN, L. M., HUNT, G. R., SALISBURY, J. W., AND BALSAMO, S. R. (1973). Compositional implications of Christiansen frequency minimums for infrared remote sensing applications. *J. Geophys. Res.* 78, 4983-5003.
- LOWMAN, P. D., JR. (1976). Crustal evolution in silicate planets: Implications for the origin of continents. *J. Geol.* 84, 1-26.
- LYON, R. J. P. (1964). *Evaluation of Infrared Spectrophotometry for Compositional Analyses of Lunar and Planetary Soils*. II. *Rough and Powdered Surfaces*. Stanford Research Institute Project NaSr-49 (04), Menlo Park, Calif.
- MCCORD, T. B., ELIAS, J. H., AND WESTPHAL, J. A. (1971). Mars: The spectral albedo (0.3-2.5 μ) of small bright and dark regions. *Icarus* 14, 245-251.
- MCCORD, T. B., AND WESTPHAL, J. A. (1971). Mars: Narrow-band photometry, from 0.3 to 2.5 microns, of surface regions during the 1969 apparition. *Astrophys. J.* 168, 141-153.
- MOROZ, V. I. (1976). Structure of the Martian soil from optical and infrared observations. *Kosmicheskie Issled.* 14, 85-96.
- MOROZ, V. I., AND KSANFOMALITI, L. V. (1972). Preliminary results of astrophysical observations of Mars from Mars-3. *Icarus* 17, 408-422.
- PANG, K., AND HORD, C. W. (1973). Mariner 9 ultraviolet spectrometer experiment: 1971 Mars' dust storm. *Icarus* 18, 481-488.
- PETERSON, J. T. (1968). *Measurement of Atmospheric Aerosols and Infrared Radiation over Northwest India and Their Relationship*. University of Wisconsin, Department of Meteorology, Tech. Note 38.
- POLLACK, J. B., AND SAGAN, C. (1967). An analysis of Martian photometry and polarimetry. Smithsonian Astrophysical Observatory Special Report 258, p. 96.
- POLLACK, J. B., AND SAGAN, C. (1969). An analysis of Martian photometry and polarimetry. *Space Sci. Rev.* 9, 243-299.
- POLLACK, J. B., TOON, O. B., AND KHARE, B. N. (1973). Optical properties of some terrestrial rocks and glasses. *Icarus* 19, 372-389.
- PROSPERO, J. M., AND BONATTI, E. (1969). Continental dust in the atmosphere of the eastern equatorial Pacific. *J. Geophys. Res.* 74, 3362-3371.
- SAGAN, C. (1973). Sandstorms and eolian erosion on Mars. *J. Geophys. Res.* 78, 4155-4161.
- SAGAN, C., AND BAGNOLD, R. A. (1976). Fluid transport on Earth and aeolian transport on Mars. *Icarus* 26, 209-218.
- SAGAN, C., AND POLLACK, J. B. (1967). Anisotropic, nonconservative scattering and the clouds of Venus. *J. Geophys. Res.* 72, 469-477.
- SAGAN, C., TOON, O. B., AND GIERASCH, P. (1973). Climatic change on Mars. *Science* 181, 1045-1049.
- SAGAN, C., VEVERKA, J., AND GIERASCH, P. (1971). Observational consequences of Martian wind regimes. *Icarus* 15, 253-278.
- SALISBURY, J. W., AND HUNT, G. R. (1969). Compositional implications of the spectral behavior of the Martian surface. *Nature* 222, 132-136.
- SCHÜTZ, L., AND JAENICKE, R. (1974). Particle number and mass distributions above 10^{-4} cm

- radius in sand and aerosol of the Sahara desert. *J. Appl. Meteorol.* **13**, 863-870.
- SINTON, W. M. (1967). On the composition of the Martian surface materials. *Icarus* **6**, 222-228.
- SMITH, R. N., YOUNG, D. A., SMITH, E. N., AND CARTER, C. C. (1963). The structure and properties of carbon suboxide polymer. *Inorganic Chem.* **2**, 829-838.
- SPITZER, W. G., AND KLEINMAN, D. A. (1961). Infrared lattice bands of quartz. *Phys. Rev.* **121**, 1324-1335.
- TOON, O. B. (1975). Climatic change on Mars and Earth. Thesis, Cornell University.
- TOON, O. B., AND POLLACK, J. B. (1976). A global average model of atmospheric aerosols for radiative transfer calculations. *J. Appl. Meteorol.* **15**, 225-246.
- TUDDENHAM, W. M., AND LYON, R. J. P. (1960). Infrared techniques in the identification and measurements of minerals. *Analyt. Chem.* **32**, 1630-1634.
- TUDDENHAM, W. M., AND STEPHENS, J. D. (1971). Infrared spectrophotometry. In *Modern Methods of Geochemical Analysis*. (R. E. Wainerdi and E. A. Uken, Eds.). Plenum, New York.
- WEAST, R. C. (1966). *Handbook of Chemistry and Physics*. Chemical Rubber Co., Cleveland, Ohio.
- WINDOM, H. L. (1969). Atmospheric dust records in permanent snowfields; implications to marine sedimentation. *Geol. Soc. Amer. Bull.* **80**, 761-782.
- WOOD, J. A. (1963). Physics and chemistry of meteorites. In *Moon Meteorites and Comets* (B. M. Middlehurst and G. P. Kuiper, Eds.), pp. 337-401. University of Chicago Press, Chicago.
- YAMAMOTO, G., TANAKA, M., AND KAMITANI, K. (1966). Radiative transfer in water clouds in the 10-micron window region. *J. Atmos. Sci.* **23**, 305-313.
- ZERULL, R., AND GIESE, R. H. (1974). Microwave Analog Studies. In *Planets, Stars and Nebulae Studied with Photopolarimetry* (T. Gehrels, Ed.) pp. 901-914. University of Arizona Press, Tucson.